Author

Meredith E. Dennis

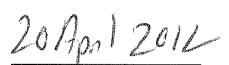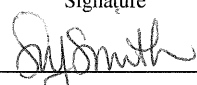**Title**
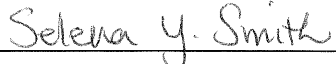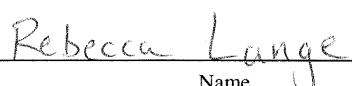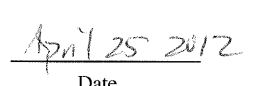
Regional paleovegetation records of the Eocene-Oligocene transition of Montana

submitted in partial fulfillment of the requirements for the degree of
Master of Science in Geology
Department of Earth and Environmental Sciences
The University of Michigan
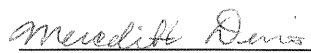
Accepted by:

_____	Naḷḷ-r D. Shḷḷ-	20 April 2012
Signature	Name	Date
_____	Selena y. Smith	April 20 2012
Signature	Name	Date
_____	Rebecca Lange	April 25 2012
Department Chair Signature	Name	Date

I hereby grant the University of Michigan, its heirs and assigns, the non-exclusive right to reproduce and distribute single copies of my thesis, in whole or in part, in any format. I represent and warrant to the University of Michigan that the thesis is an original work, does not infringe or violate any rights of others, and that I make these grants as the sole owner of the rights to my thesis. I understand that I will not receive royalties for any reproduction of this thesis.

☑ Permission granted.

☐ Permission granted to copy after: _____

☐ Permission declined.

_____
Author Signature

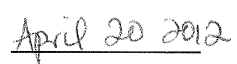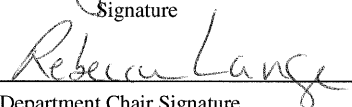**Earth and Environmental Sciences**
UNIVERSITY OF MICHIGAN
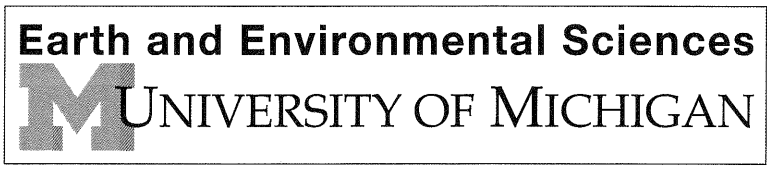
REGIONAL PALEOVEGETATION RECORDS OF THE EOCENE-OLIGOCENE TRANSITION OF MONTANA

Meredith E. Dennis[1], Nathan D. Sheldon[1], and Selena Y. Smith[1]

[1]*Department of Earth and Environmental Sciences, University of Michigan, 2534 C.C. Little Science Building, 1100 North University Ave, Ann Arbor MI 48109-1005*

Abstract

The climate change that occurred over the Eocene-Oligocene transition (EOT; ~33.7 Ma) is the most significant and dramatic of the Cenozoic, reflecting a change from "hothouse" to "icehouse" conditions. Paleoclimate and paleovegetation studies over the last 50 years have put together a broad picture of vegetation change in southwestern Montana. Although general predictions concerning biome response to climate change are useful, a refined understanding is necessary to forecast the effects of future anthropocentric climate change. This study investigates five sites in southwestern Montana (North Hough Draw, Little Spring Gulch, Big Stonerpipe, Little Pipestone, and Matador Ranch) using geochemical analyses of fossilized soils (paleosols) in combination with plant biosilica (phytoliths) to infer the regional response of vegetation during the EOT. In contrast with the marine record of the EOT, whole rock geochemical analyses indicate little change in mean annual temperature and precipitation. Phytoliths from the five sites are indicative of a forested or woodland landscape with a small component of (likely understory) grasses (~22.1%). The most significant vegetation change occurs in regard to the percentage of open-habitat grasses at each site, with a clear increase in open habitat grasses around 34.5 Ma, followed by a return to a more heavily forested landscape over the EOT. Stable carbon isotope data from organic carbon inclusions in paleosols change in tandem with the abundance of open-habitat grasses, and indicate that open-habitat grasses became more abundant as drier conditions prevailed. These results affirm findings of lower resolution studies of

southwestern Montana, suggest a long-term, gradual cooling and drying trend over the EOT, and highlight the importance of local geography as a predictor of response to climate change.

1. Introduction

While we can predict broadly how biomes will respond to climate change, to make the most accurate predictions of vegetation response to future climatic change, we need to understand localized responses to global changes and how regional climate and topography impact biotic change. The climate change that occurred over the Eocene-Oligocene transition (EOT; ~33.7 Ma) is the most significant and dramatic of the Cenozoic, reflecting a change from "hothouse" to "icehouse" conditions (Miller et al., 1987; Zanazzi et al., 2007). While the consensus view is that global climate became cooler and drier during the EOT, intermontane continental basins were less impacted by global EOT climate fluctuations than lower paleoelevation or near-coastal sites (Sheldon and Retallack, 2004; Sheldon, 2009), or than marine records (e.g., Liu et al., 2009). These broad climate reconstructions, in conjunction with paleobotanical studies, can be used to infer paleovegetation. This paper uses geochemical analyses of fossilized soils (paleosols) in combination with plant biosilica (phytoliths) to investigate the regional response of vegetation in southwestern Montana during the EOT.

1.1 Global Paleoclimate Record of the EOT

Between the late Paleozoic and the EOT, the Earth was virtually ice free (Tripati et al., 2008). Evidence of ephemeral ice sheets at the poles in the Eocene prior to the EOT suggests that Milankovitch cycles were the driver rather than global cooling events (Miller et al., 2005). This is supported by evidence for warm ocean surface temperatures at high latitudes (>10-20°C;

Miller et al., 2005; e.g., North Atlantic, Liu et al., 2009). After the Early Eocene, global climate began cooling and drying slowly, a trend which produced the modern hydrospheric conditions characterized by ice caps on both poles (Zachos et al., 2001). However, this trend was not uniform, and was punctuated by the accumulation of northern hemisphere ice during the Oi-1 glaciation and a brief warm and wet interval in the Middle Miocene (Zachos et al., 2001).

The marine record of climate change during the EOT based on oxygen isotope (δ^{18}O) records indicates a rapid and dramatic climate shift (Coxall et al., 2005; Pearson et al., 2009), though interpretation of isotopic records is complicated by the fact that δ^{18}O responds both to changes in temperature, salinity, and ice volume. Independent temperature proxy records from biomarkers (alkenone unsaturation and tetraether indices) indicate ~5°C cooling (Liu et al., 2009), which suggests that perhaps half of the oxygen isotopic signature is due to icesheet growth rather than to temperature change. This finding has been corroborated by some continental studies of fossil tooth enamel and bone (>8°C cooling; Zanazzi et al., 2007), but those results need to be considered carefully given that fossil bone is generally thought to be unreliable as a paleoclimate proxy (e.g., Sheldon, 2009) and that independent records based on paleosols and paleofloral results from the same locations indicate little climatic change (Terry, 2001; Sheldon and Retallack, 2004).

Alternatively, gradual cooling and drying is supported by marine studies of fish otoliths (Ivany et al., 2000) and marine Mg/Ca ratios (Lear et al., 2000), which indicate little cooling over the EOT. Freshwater and terrestrial paleoclimate analyses support a more gradual change as well. Oxygen isotopes from tooth enamel, gastropod shells, gyrogonites and otoliths from the Isle of Wight, UK suggest little change in summer temperature due to the Oi-1 glaciation (Grimes et al., 2005). Paleosol studies based on depth to the calcic horizon and degree of

chemical weathering in the Ebro Basin, Spain (Sheldon et al., 2012) as well as Oregon, Montana, and Nebraska, USA (Sheldon and Retallack, 2004) similarly indicate a long-term, gradual cooling/drying.

Hypotheses to explain the EOT invoke a myriad of causal mechanisms including changing ocean circulation and continent rearrangement (Raymo et al., 1992), atmospheric thermal redistribution from mountain uplift (Raymo et al., 1992), and the reduction of atmospheric CO_2 (Retallack, 2001; Tripati et al., 2008; Pearson et al., 2009). The latter explanation is currently viewed as the most likely, although effects of the other processes should not be ignored (DeConto et al., 2008). Recent results using a boron isotope pH proxy to estimate pCO_2^{atm} before, during, and after the EOT support the role of declining CO_2 in Antarctic ice sheet growth, with a significant dip in pCO_2^{atm} prior to the EOT (Pearson et al., 2009). DeConto et al. (2008) used oxygen isotopes and the effects of orbital forcing to model pCO_2^{atm} thresholds for Antarctic glaciation. In line with Pearson et al.'s (2009) finding of a central pCO_2^{atm} value of 760 ppm, DeConto et al.'s (2008) study predicted Antarctic glaciations below ~750 ppm . Furthermore, as little evidence exists for continental Northern Hemisphere ice sheets, it appears as though Antarctic ice growth alone is sufficient to explain the oxygen isotope excursion observed at the boundary (DeConto et al., 2008).

1.2 *Geologic History of Southwestern Montana*

Modern southwestern Montana is composed of one central basin—the Dillon-Renova Basin—surrounded by the Snake River Plain to the south and volcanic highlands on all other sides (Fritz et al., 2007). The Dillon-Renova Basin is divided into a series of smaller basins that are the result of Basin-and-Range style faulting (Fields et al., 1985). Each of these smaller basins contains a thick record of continental Cenozoic sediment (Tabrum et al., 1996) that is divided

into two main formations divided by an angular unconformity: the Renova Formation (middle Eocene-early Miocene) and the Sixmile Creek Formation (middle Miocene to late Pliocene) (Fields et al., 1985; Fritz et al., 2007). Both formations lie unconformably atop late Cretaceous sediments. According to Fritz et al. (2007), the Renova Formation formed as a continuous wedge of sediment, which was then broken up in the middle Miocene into the grabens, where the Sixmile Creek sediments accumulated. There is no clear lithologic boundary between the Renova and Sixmile Creek Formations, with the main distinguishing feature being the finer grain size of the Renova Formation relative to the Sixmile Creek Formation. In the absence of long, continuous sections, local chronology in the Dillon-Renova Basin has relied on the extensive faunal record (Fields et al., 1985; Tabrum et al., 1996).

1.3 Fauna: Worldwide and Local Records

Beginning in the Middle Eocene, North American fauna underwent a series of culling events—extinctions on both land and sea of which the EOT (34.2-33.7 Ma) was prominent (Hutchison, 1992). Warm-water gastropods around Mexico peaked in diversity just prior to the Middle Eocene (Squires, 2003), but were subsequently replaced by immigrant mid-latitude taxa that were escaping the dropping temperatures observed closer to the Oligocene (Prothero, 1994). Terrestrial fauna were likewise influenced by cooling and drying climate conditions, albeit less dramatically than marine fauna (Hutchison, 1992). Subtropical land snails, reptiles and amphibians common at mid-latitudes during the Chadronian were replaced with drought-hardy varieties by the Orellan (Evanoff et al., 1992 in Prothero, 1994). In southwestern Montana, local fauna over the EOT have been characterized by their provincialism, with 20–40% of known mammalian species being endemic to the region (Tabrum et al., 1996). In Europe, this time

period is known as the Grande Coupure or "great cutoff" and likewise corresponds to significant extinctions and turnover around 33.2 Ma (Hooker et al., 1995; 2009).

1.4 Flora

As the North American climate cooled and dried toward the EOT, the vegetation shifted from subtropical, broad-leaved evergreen forests to more open mixed coniferous and broad-leaved deciduous forest (Wing, 1987; Tiffney et al., 2001). For the majority of the Eocene, North America was covered with the former vegetation types with two main exceptions: 1) dry areas of the eastern Rocky Mountains may have supported islands of deciduous vegetation and 2) uplands in the western Rockies that may have likewise supported cooler-adapted deciduous vegetation (Wing, 1987). The development of these uplands played a major role in the development of North American floras as it broke up a formerly continuous lowland between the Rocky Mountains and the West Coast (Wing, 1987). As with subtropical land snails and marine gastropods, tropical and paratropical vegetation in the northern Rocky Mountains and High Plains which had formerly existed at high latitudes (60–65°N) began to be replaced by cool-tolerant deciduous communities closer to the EOT (Graham, 1999).

In line with the transition to a cooler, drier climate, Late Eocene (Chadronian) paleovegetation from Nebraska including woodlands of *Robinia, Prunus* and *Zelkova* suggest a seasonal climate, while root diameters and tree spacing from the Badlands of South Dakota indicate a large drop in precipitation, from 1000 mm yr^{-1} in the late Middle Eocene (38 Ma) to between 250–450 mm yr^{-1} during the Late Oligocene (29.5 Ma) (Sheldon and Retallack, 2004). Vegetation patterns due to this precipitation change are expected to have transitioned from moist forests in the Late Eocene to an open savanna-like ecosystem by the Late Oligocene (Graham, 1999). Tanai and Wolfe (1977) used plant megafossils to characterize a wide variety of

community types from the Paleogene-Neogene in western North America, including flood-plains and humid forests, mixed deciduous-coniferous forests, shoreline communities, a high montane forest, and a subhumid chaparral.

Several Chadronian and Orellan-aged plant megafossil assemblages have been described from southwest Montana (Becker, 1960, 1969, 1972, 1973; Wing, 1987; Graham, 1999). The Beaverhead Basin floras (Chadronian; Christensen Ranch, Horse Prairie, and Medicine Lodge florules; Becker, 1969) were interpreted as subhumid, mixed coniferous and broad-leaved deciduous forests. Fabaceae are the most diverse family, followed by Rosaceae and Rhamnaceae (Becker, 1969). Many modern genera are present, including *Juniperus*, *Quercus, Mahonia, Acer,* and *Salix*, as well as a less prominent presence of *Abies, Picea, Betula, Cassia*, *Cercocarpus, Fraxinus*, and *Zelkova* (Graham, 1999). Also known from this time period are floral elements currently found in eastern North America, western North America, and Asia, including *Ginkgo, Glyptostrobus, Metasequoia, Ailanthus,* and *Eucommia*.

In the Upper Ruby River Basin of southwestern Montana, the Mormon Creek, York Ranch, and Metzel Ranch floras (Becker, 1960, 1972, 1973) are dated as Orellan (Wing, 1987) while the Ruby paper shales (Becker, 1961) are considered to be Whitneyan (Wing, 1987). These floras resembled each other and represent temperate to dry-temperate mixed coniferous and broad-leaved deciduous forest with shrublands (Wing, 1987). The Mormon Creek flora has been characterized as a deciduous lowland with a high proportion of *Salix, Populus*, *Cercidipyllum*, and *Quercus* under humid, temperate conditions (Becker, 1960). Prominent taxa of the Metzel Ranch flora included members of the Rosaceae and Fabaceae, as well as a lesser presence of *Juniperus,* Gramineae, *Crataegus*, and *Mahonia*—a group of taxa indicative of dry conditions (Becker, 1972). The Metzel Ranch flora differed from the Beaverhead flora in having few

gymnosperms and lacking oaks. In contrast with these deciduous, subhumid plant communities, the York Ranch flora appears to have been dominated by floodplain and riparian elements that bear strong resemblance with floras from modern northeastern North America, but also included elements of western and southwestern North American and Asian floras (Becker, 1973). Prominent families included Salicaceae, Rosaceae, Ulmaceae, and Betulaceae. Graham (1999) observed that none of the paleovegetation from southwestern Montana showed a distinct climatic trend and that all communities from the EOT displayed mixed coniferous and broad-leaved deciduous forest and shrubland amid temperate to dry-temperate conditions. MAP (mean annual precipitation) estimates using CLAMP put temperature during this interval between 11–12°C with a seasonal range of 16°C (Graham, 1999).

2. Methods

2.1 Sample Collection

Samples for geochemical analysis or phytolith extraction were analyzed from five dated localities in southwestern Montana from the Climbing Arrow Member of the Renova Formation in the Sage Creek Basin (Figure 1). Age-dating is based on North American Land Mammal Ages (NALMA) for vertebrate sites compiled in Nichols and Hanneman (2001), and on radiometric dates compiled in Fritz et al. (2007) and Retallack (2007). Each locality was logged stratigraphically excluding Little Pipestone (which was previously logged by Sheldon and Hamer, 2010), and in instances of short stratigraphic sections (<10 m), multiple sections were logged and correlations between sections were made based on lithology. Lateral samples were also taken where clearly continuous lateral beds were present. All samples were collected from trenches dug to a depth of 10–20 cm to minimize modern contamination. Paleosols (n=37) were identified based on the presence of root traces, burrows, and/or mottled coloring. In the absence

of paleosol identifications, samples were taken at each meter level to ensure temporal coverage. Paleoclimate and paleoenvironmental interpretations are based on physical characteristics of the paleosols (i.e., mottling, pedotype), degree of chemical weathering, and carbon isotopic composition of organic matter (i.e., root traces). Pedological, geochemical, and isotope data are compiled in Tables 1, 2, and 3-4, respectively.

2.2 Whole Rock Geochemistry

Subsoil horizons (B horizons), characterized by the presence of mottling (Bw) or gleying (Bg), accumulate material washed out of the topsoil horizon and contain valuable paleoclimate proxy information (Retallack, 2001). Geochemical analyses were performed at ALS Chemex (Vancouver, Canada) on Bw or Bg horizons (n=20) to provide inputs for several geochemical proxies that estimate mean annual temperature (MAT), mean annual precipitation (MAP), and by extension, degree of chemical weathering (CIA-K; Sheldon et al., 2002). Soils that form under higher precipitation rates and warmer temperatures are more heavily weathered. A relationship between weathering and MAP in modern soils was derived by Sheldon et al. (2002) and is given by the equation:

$$P = 221e^{0.0197(\text{CIA-K})} \tag{1}$$

where CIA-K is the chemical index of alteration without K (to minimize the effects of potassium metasomatism; Maynard, 1992). The CIA-K is related to paleoprecipitation per Eq (1), where R^2 = 0.72 with a standard error of ± 182 mm yr^{-1} (Sheldon et al., 2002). Cooler climates tend to accumulate higher ratios of potash and soda in comparison with alumina in their soils and a climofunction has been established for this relationship as well:

$$T = -18.5(S) + 17.3 \tag{2}$$

where S is the ratio of Na_2O and K_2O to Al_2O_3 (Sheldon et al., 2002), with an $R^2 = 0.37$ and a standard error of ±4°C. Results from both have been corroborated by independent paleobotanical and paleopedological proxies (see examples in Sheldon and Tabor, 2009), with Eq (1) being quantitatively comparable and Eq (2) recording the vector of change appropriately, while typically underestimating MAT relative to other proxies.

2.3 Stable Isotope Preparation

Samples for stable organic carbon isotope analysis (n=18) were washed with methanol and dried overnight. Carbonate was digested with repeated washes in 7.0% HCl on a hot plate (50°C), for up to 45 minutes. Samples were then rinsed with DI water at 40°C for 20 minutes, up to three times. Samples were dried, crushed, and placed into crimped tin capsules for analysis using a Costech Elemental Analyzer attached to a Delta V+ isotope ratio mass spectrometer at the University of Michigan Stable Isotope Laboratory. Results were calibrated using international standards (IAEA600, IAEACH-6) and are given in delta notation relative to the V-PDB. Analytical uncertainty was <0.08‰ for $\delta^{13}C_{org}$. Stable isotope data are compiled in Tables 3 and 4.

2.4 Phytolith Extraction

Phytolith extraction followed the methods of Strömberg (2007). Approximately 100 g of sample (n=70) was homogenized, and a 1.0 g subsample was analyzed for phytoliths. Subsamples were crushed into sand-sized pieces with a mortar and pestle. Concentrated (37.0%) HCl was added to remove carbonate, after which samples were rinsed with deionized (DI) water and sieved to remove the coarse (>250 μm) fraction. Organic material was removed with a solution of nitric acid (HNO_3) and potassium chlorate ($KClO_3$; Schultze's solution). Samples were left in the Schulze's solution in a hot water bath and stirred every ten minutes for 45–60

minutes. Samples were again rinsed with DI water and sieved through a 53 μm sieve to deflocculate clay minerals. Samples were rinsed and centrifuged to remove clays. Phytoliths were extracted by heavy liquid floatation using zinc bromide ($ZnBr_2$) with a specific gravity of 2.38 g cm^{-3}.

2.5 Vegetation analysis

Samples with good to high phytolith yields (>1.0% of silica in five fields of view) of moderately to well-preserved phytoliths (qualitatively characterized by degree of brokenness, abrasion, etching, etc. of silica) were dried, and subsamples of the residue mounted onto slides (two slides per sample: one using Cargille Meltmount®, refractive index = 5.39, and one using Cargille Non-Drying Immersion Oil Type A). Slides were analyzed on a petrographic microscope (400–1000x) and morphotypes were categorized based on the work of Strömberg (2003; Data Repository 1–7). Each morphotype is assigned to a plant functional type category: general forest indicators (FI-GEN), conifer/monocot (CONI/MONO), woody dicotyledons (DICOT-WO), general dicotyledons (DICOT-GEN) diagnostic palms (PALM-D), diagnostic/non-diagnostic pooid grasses (POOID-D/POOID-ND), sedges (SEDGE) or other (OTH) following Strömberg (2003; 2004; 2005; Data Repository 1, 2). For vegetation analysis, relative percentages of grass silica short cells (GSSCs = BAMB/B + POOID-D + POOID-ND + CHLOR + OTHG; Strömberg, 2004) and forest indicators (FI total = DICOT-WO + DICOT-GEN + FI-GEN + PALM-D + CONI; Strömberg, 2004) were used. Non-diagnostic grass morphotypes (NDG) and non-diagnostic (OTH) and unclassified phytoliths were excluded from final vegetation analysis based on the wide range of plant types they can come from (Strömberg 2007). Phytolith morphotypes were counted from random transects across 22 x 40 mm area. To minimize error and capture an accurate reflection of morphotype diversity, a minimum of 200

total diagnostic morphotypes were counted from each sample (Strömberg, 2009). Personal counting standard deviation based on five recounts of one sample yielded an average deviation of 3.7%, with a deviation for FIs of 5.8%, and for GSSCs of 2.1%. Phytolith results were recorded as raw counts (Data Repository 3, 4), percent of the total biosilica (Data Repository 5), as percent of total phytolith population (Data Repository 6), and as percent of FI and GSSC morphotypes for total FI+GSSC (as used for vegetation reconstruction; Data Repository 7). Average values of FIs and GSSCs for each locality were also calculated (Table 5). Values reported in section 3.4 are as percent of total phytolith population unless otherwise indicated.

3. Results

3.1 Site Descriptions

3.1.1 North Hough Draw #1

The North Hough Draw section (Figure 1; N44$^°$45'17.8", W112$^°$34'45.2"; ±4 m) is located northeast of Dell, Montana off of Sage Creek Road. Rocks from this site have been dated as Mid-Late Chadronian (Nichols and Hanneman, 2001) and were composed of siltstones and sandstones with occasional layers of $CaCO_3$ cementation (Figure 2C; Figure 3). Based on its close proximity to Little Spring Gulch (Figure 1), and the consistently different geochemistry of the two sites (Figure 5) we are inclined to place North Hough Draw closer to Mid-Chadronian, and Little Spring Gulch closer to Late-Chadronian. The *Con Color* and *Santo Hoyo* pedotypes (see section *3.2* for pedotype descriptions) were found here. The measured section was 16.5m thick, but an additional 15 m of covered section remained above this and 8–10 m of covered section below.

3.1.2 Little Spring Gulch

The Little Spring Gulch site (Figure 1; N 44°50'17.3", W112°35'54.9"; ±4 m) is ca. 12 miles to the northeast of Dell, Montana. Little Spring Gulch is composed lithologically of alternating layers of silty sandstone and fine grained sandstone (Figure 2A; Figure 3) and contains both the *Con Color* and *Santo Hoyo* pedotypes. Two sections, "A" and "B" (17.5 and 14.5 m, respectively) were measured and laterally correlated. Little Spring Gulch A and B are treated as one locality, "Little Spring Gulch." The samples from Little Spring Gulch are dated to the Mid-Late Chadronian (Nichols and Hanneman, 2001).

3.1.3 Big Stonerpipe

The Big Stonerpipe site is east of the junction between Montana Highway 2 and Montana Highway 41 (Figure 1; N45°50'35.7", W112°15'20.5"; ±3 m). Big Stonerpipe has been dated to the latest Eocene-earliest Oligocene (age assignment from Retallack, 2007). Three sections were measured at Big Stonerpipe (13.3 m, 3.8 m and 4.9 m) that were all characterized by the presence of reworked ash in at least one (but usually many) layers (Figure 3). *Taenidium* burrows and zeolites were also common features, as well as evidence of fluvial channels in nearby outcrops. The *Con Color* and *Santo Hoyo* pedotypes were found here (Figure 2D).

3.1.4 Little Pipestone

Little Pipestone is also east of the junction between Montana Highway 2 and Montana Highway 41 (Figure 1; N45°50'33.6", W112°15'40.8"; ±5 m) and is located directly across the road from Big Stonerpipe. It is a well-known vertebrate paleontology site (Douglass, 1905) and is dated as latest Eocene-earliest Oligocene (age assignment from Retallack (2007) and Sheldon and Hamer (2010)). It consists of claystones, siltstones, and sandstones with sedimentary structures indicative of fluvial channels (Figure 2E; Figure 3). Pedotypes described by Sheldon and Hamer

(2010) include the equivalent of the *Con Color* and *Santo Hoyo* pedotypes. See Sheldon and

Hamer (2010) for full stratigraphic description.

<u>3.1.5 Matador Ranch</u>

The Matador Ranch site (Figure 1; N44°45'1", W112°33'59.7"; ±4 m) is 8.8 miles to the

northeast of Dell, Montana. Samples from the Matador Ranch locality are characterized by fine

silty sandstones at the base coarsening up to fine-medium grained sandstone (Figure 2B; Figure

3). The *Con Color* and *Anegado* Pedotypes were present here, but the *Santo Hoyo* Pedotype was

not, in spite of the presence of trace burrows. The described section was 81.9 m and has been

dated to the middle Orellan age (Tabrum et al., 1996).

3.2. Pedotypes

3.2.1 Pedotype "Con Color"

The "*Con Color*" paleosol crops out in each of the five described sections (Matador Ranch,

North Hough Draw, Little Spring Gulch, Little Pipestone, and Big Stonerpipe), and is

comparable to a modern Inceptisol (Table 1; Soil Survey Staff, 2003). It contains both A and Bw

horizons and is characterized by moderate to weak mottling including light greenish gray (8/1,

Gley 1), to pale/very pale brown (6/3, 10YR; 8/2, 10YR) and light reddish brown mottles (7/3,

2.5YR; Munsell Soil Color Chart, 2000). Parent material included sandy or clayey silt and is

representative of a seasonally flooded/disturbed landscape (i.e., floodplain).

3.2.2 Pedotype "Anegado"

The "*Anegado*" paleosol appears at Matador Ranch and is comparable to a modern Inceptisol

(Table 1; Soil Survey Staff, 2003). It contains both A and Bg horizons and is characterized by

gleyed, but not mottled horizons. The parent material is silt or sandy silt and represents a more continuously waterlogged site.

3.2.3 Pedotype "Santo Hoyo"

The "*Santo Hoyo*" paleosol appears at Little Spring Gulch, North Hough Draw, Big Stonerpipe and Little Pipestone. It is comparable to a modern Entisol (Table 1; Soil Survey Staff, 2003) and is characterized by very weak or absent soil development with either root traces, burrows, or both, but no horizonation. The parent material ranges from silt with quartz pebbles to medium/fine sand and represents an infrequently disturbed and drier landscape.

3.3. Geochemical Analyses

3.3.1 Weathering Intensity

Changes in the degree of chemical weathering of paleosol Bg horizons are indicated as the Chemical Index of Alteration minus potassium (CIA-K). The range of values measured from our sections is 56.1–74.2 with a mean of 63.3 ($\sigma = 4.4$; Table 2). A more subtle weathering relationship is present in the molecular ratio of barium/strontium (BaO/SrO; Vinogradov, 1959), which characterizes the degree of leaching experienced by a soil or paleosol. The trend observed in the BaO/SrO relationship is broadly similar to that of the CIA-K with some exceptions. Namely, the two samples taken from Big Stonerpipe have the highest CIA-K values (indicative of strong weathering), but the lowest BaO/SrO ratios (indicative of little leaching; Figure 5). This may be explained by the higher quantities of NaO compared to other sample localities, which is known to increase the solubility of strontium salts (Vinogradov, 1959).

3.3.2 Paleoprecipitation and temperature

Paleoprecipitation can be estimated based on the lack of pedogenic carbonate formation in paleosols following Jenny (1941) as >800 mm yr^{-1}. Reconstructed paleoprecipitation values

using Eq (1) ranged from 675–954 mm yr^{-1}, with a mean value of 772 mm yr^{-1} ($\sigma = \pm$ 67 mm). Temperature estimates made using Eq (2) produced a temperature range of approximately 11–14°C with a mean of 12°C (σ = 0.86°C) (Table 2). These results are consistent with previous work in the region on penecontemporaneous paleosols (Retallack, 2007) as well as macrofossil estimates (Graham, 1999). In general, MAP and MAT remain steady throughout the interval, with only modest cooling and drying around 32.5 Ma (772 mm yr^{-1} to 725 mm yr^{-1} $\pm$ 29 mm; 12.29°C to 11.99°C $\pm$ 0.53°C; Figure 5).

3.3.3 Stable Isotope Results

The range of $\delta^{13}C_{org}$ is -20.31 ‰ to -24.90 ‰, with an average of -22.80 ‰ and a standard deviation of 1.44 ‰. Mean values for each sites varied slightly. North Hough Draw and Matador Ranch (the oldest and youngest sites, respectively), each had average values around -22.25 ‰ (note, Matador Ranch n =1). Little Spring Gulch, the second oldest site, had the most depleted $\delta^{13}C_{org}$ average, with -23.84 ‰, and Big Stonerpipe, the second youngest, had the most enriched value, at -21.38 ‰. The trend observed is of moderate $\delta^{13}C_{org}$ values in the mid-Chadronian, a drop in $\delta^{13}C_{org}$ during the late-Chadronian, then rebound to higher $\delta^{13}C_{org}$ during the latest-Chadronian, and finally a leveling out to pre-EOT values in the Orellan. See Table 3 and 4 for individual sample data and summary data on individual sites, respectively.

3.4. Phytoliths

Phytolith results are reported here as a percent of total phytolith population per sample, unless otherwise indicated. Phytolith results used for vegetation reconstruction are assigned FI and GSSC percents out of total FI + GSSC morphotypes only (Data Repository 7), and are discussed further in *Section 4.3*. With the exception of Matador Ranch, all sites yielded well.

Only three samples were analyzed for the Little Pipestone locality, but this locality directly corresponds to the Big Stonerpipe locality in time and location (lateral separation of ~150 m). Two samples from Matador Ranch were evaluated quantitatively, and two more were examined only qualitatively due to a low yield.

The average across all five localities for total forest indicators (FIs) was 50.2% ($\sigma =$ 8.1%) and the average percent GSSCs was 15.0% ($\sigma = 5.6\%$) (Table 5). For the most part, assemblages from all sites contained approximately the same broad categories of morphotypes, with differences in abundance being the main distinguishing characteristic (Data Repository 3, 6 and 7). All assemblages excluded Sclereid (Scl), Knobby (Kn), and most Blocky (Blo) morphotypes, which are typically diagnostic of conifers or general forest indicators (Strömberg, 2004), as well as most pyramidal (PY) and saddle (SA) morphotypes that are diagnostic of bambusoid and chloridoid grasses (Data Repository 3). In total, forty morphotypes were recorded for all samples analyzed. The average number of morphotypes per site was ~22, with a range of 16–28. The most commonly observed morphotype regardless of locality were undiagnostic "elongate" morphotypes (Elo-1; Figure 4C). Common diagnostic FI morphortypes included small pink spheres (Cl-4; Figure 4S-U), MD elongates (Elo18; Figure 4D), echinate spheres (Clm-2; Figure 4I,J), VI-1 spheres (VI-1; Figure 4K) and anticlinal epidermal cells (Epi-3; Figure 4O-P). Less commonly observed FI morphotypes included tracheary elements (Tra-1; Figure 4Q), and worm/pupa-like tracheary elements (Tra-2; Figure 4V). The most common GSSC morphotypes observed were those likely belonging to pooid grasses (CO-1, A&B; CO-2; Figure 4E,F,H; Figure 4G). Less commonly observed GSSC morphotypes included small "spiked" rondels (CO-4; Figure 4A) and collapsed saddles (SA-3; Figure 4B). Very few sponge spicules or diatoms (Figure 4L,N) – indicators of standing water – were recorded. The only site

with average "aquatic biosilica" assemblages over 1.0% of total biosilica (including all phytoliths, diatoms, chrysophytes and sponge spicules) was Matador Ranch, with 1.7%. Two of the highest aquatic biosilica yielding samples from Matador Ranch were the two poorest yielding for phytoliths and were included only qualitatively in vegetation analysis. Only one other sample, also from Matador Ranch, had an aquatic biosilica content higher than 9.5% (Data Repository 5).

Eocene localities: North Hough Draw, Little Spring Gulch, Big Stonerpipe, and Little Pipestone of the Renova Formation.

3.4.1 North Hough Draw

The North Hough Draw locality (n=6) had the second highest percentage of FIs (mean=54.4%) ranging from 38.6–81.7% (Data Repository 6, Table 5). The majority of FIs at North Hough Draw came from anticlinal epidermal cells (Epi-3). Other FI morphotypes included echinate spheres (Clm-2; palms), small pink spheres (Cl-4), MD elongates (Elo-18), and thick trapezoidal rectangles with knobs (Blo-7). Rarely observed morphotypes included tracheary elements (Tra-1, Tra-2, and Tra-7), sinuate elongates (Elo-20), faceted regular plates (Blo-3), and VI-1 spheres.

North Hough Draw was composed of 9.2% GSSCs, with individual samples ranging from 4.0–17.5% of the total phytolith population. Rondels (CO-1 Type A & B, CO-2) indicative of pooid grasses were the most common. Less frequently observed morphotypes also included keeled rondels (KR-1), conical rondels with concave bases (COF-5; all indicative of pooid grasses), tall rondels with spiked tops (COF-1) or concave plates (COF-6), and Bl-13 (all

bambusoid grasses) (Data Repository 3 and 5). As with the other sites, no clear pattern was distinguishable with regard to time or lithology.

3.4.2 Little Spring Gulch

The Little Spring Gulch site (n=9) contained a mean FI of 42.5%, with individual samples ranging from 16.0–61.5% (Data Repository 6, Table 5). The most common FI morphotypes included anticlinal epidermis cells (Epi-3), smooth spheres with concentric laminations (VI-1), echinate spheres (Clm-2) typical of palms, small pink spheres (Cl-4), tracheary elements (Tra-1, Tra-2), and MD elongates (Elo-18) (Figure 4; Data Repository 3). None of these morphotypes were present in all nine samples. The biggest disparity appeared among the small pink spheres and the echinate spheres. In four of the nine samples Cl-4 was >25.0% of the total FIs, while the other five samples had 0.0–0.1% Cl-4. Likewise, one sample contained 35.5% echinate spheres, while four others contained almost 0.0%.

The Little Spring Gulch site the second highest percentage of GSSCs (mean=20.3%) with a range of 2.0–55.2% of total phytoliths (Table 5; Data Repository 6). Most GSSC morphotypes came from 2–3 specific morphotypes. All samples included general truncated rondels (CO-1, A & B), suggestive of pooid grasses, and truly conical rondels (CO-2), diagnostic of pooid grasses. Other rare morphotypes included *Chusquea* rondels (CO-3); small, irregular pyramidal bodies (PY-2; bambusoid grasses); keeled rondels (KR-1; pooid grasses); and true saddles (SA-1; chloridoid grasses). Sedges (Epi-6) were rare, but present, as observed on cursory scans. Overall, variation among samples was present for both FIs and GSSCs, but no discernible trend was evident among the samples at this site.

Lateral samples from Little Spring Gulch were also analyzed. Two samples were processed, approximately 30 m to the left and right of the main section. The main section sample

(LSGB11-11) was composed of 61.5% FIs and 4.0% GSSCs (Data Repository 6). The average of the two lateral samples yielded 62.0% FIs ($\sigma = 3.7$), and 22.9% GSSCs ($\sigma = 1.4$), of which the FI average is significantly different by more than two standard deviations (Table 5). The Little Spring Gulch lateral samples had the highest percentage of both FI and GSSC morphotypes out of any other locality. Common FI morphotypes were the same as those from the main Little Spring Gulch section: anticlinal epidermis cells (Epi-3), smooth spheres with concentric laminations (VI-1), echinate spheres (Clm-2), small pink spheres (Cl-4), tracheary elements (Tra-1, Tra-2), and MD elongates (Elo-18). GSSC morphotypes were also largely similar to those found in the main section, but with the addition of rare tall rondels with spiked tops (COF-1), keeled rondels (KR-1), and saddle morphotypes (SAF-1, SA-1 and SA-5) diagnostic of chloridoid grasses (Data Repository 3). The lateral samples likewise showed no trend with respect to time or lithology.

3.4.3 Big Stonerpipe

The Big Stonerpipe locality had an average of 40.5% FIs with a range of 14.9–68.6% (Data Repository 6, Table 5). Major constituents were small pink spheres (Cl-4), with small numbers of tracheary elements (Tra-1, Tra-2), VI-1 spheres and MD elongates (Elo-18) also observed. Very rare morphotypes included anticlinal epidermal cells (Epi-3), sinuate elongates (Elo-20), and multifaceted S-bodies (Scl-3) (Data Repository 3).

GSSCs at Big Stonerpipe comprised 12.7% of the assemblage (range = 3.2–23.2%). The Big Stonerpipe locality showed the most diversity among GSSCs, although the vast majority of morphotypes were the general conical rondels (CO-1, Type A & B; indicative of pooid grasses) (Data Repository 6). Other morphotypes included truly conical rondels and keeled rondels (pooid grasses) (CO-2 and KR-1, respectively); collapsed saddles (SA-3), *Chusquea* rondels (CO-3) and

tall rondels with spiked tops (COF-1; bambusoid grasses) and true saddles (SA-1) and saddles with one indented side (SA-5; chloridoid grasses). Sedge (Epi-6) morphotypes were also exceedingly rare, but observed (Data Repository 3). Variation in abundances of FI and GSSC morphotypes existed, but no clear pattern was observed overall.

3.4.4 Little Pipestone

The Little Pipestone locality (n=3) had a high percentage of FIs (mean=52.2%; Table 5). Total FIs ranged from 25.0–75.3% among samples (Data Repository 6). Small pink spheres (Cl-4) comprised, on average, 85.0% of the FIs, but anticlinal epidermal cells (Epi-3), tracheary elements (Tra-1, Tra-2), echinate spheres (Clm-2) and VI-1 spheres were also observed universally. Other, rarely observed morphotypes included the epidermal plates of sedges (Epi-6), MD elongates (Elo-18), and multifaceted S-bodies (Scl-3) (Data Repository 3).

Little Pipestone contained the third highest percentage of GSSCs (mean=16.5%), and one of the smallest ranges (14.2–22.9%). The biggest constituent of the GSSCs were the generic truncated rondels (CO-1, Type A & B; 71.8%), but small "spiked" and keeled rondels (CO-4 and KR-1, respectively) were also observed, both of which are also indicative of pooid grasses. The Little Pipestone site had the highest percentage of true saddle morphotypes (SA-1), and was the only location with "indented" saddles (SA-5), both of which are indicative of chloridoid grasses. Other very rarely observed morphotypes included *Chusquea* rondels (CO-3), tall conical rondels with concave plates (COF-6), collapsed saddles (SA-3), and tall rondels with spiked tops (COF-1; bambusoid grasses) (Data Repository 3 and 5). No clear pattern in vegetation was observed for either FI or GSSC morphotypes with regard to time or lithology.

3.4.5 Oligocene localities: Matador Ranch of the Renova Formation

The only Oligocene locality sampled was also by far the poorest yielding site. Of approximately 33 samples taken, only six yielded sufficiently well-preserved phytolith assemblages to further analyze. Of those six, only two produced over 200 diagnostic morphotypes, while two more were evaluated qualitatively. The average percent of FIs in the top yielding samples was 49.1% of the total phytolith population, with individual samples ranging from 41.0–57.0% (Data Repository 6, Table 5). The most common FI morphotypes were the echinate spheres (Clm-2; palms), small pink spheres (Cl-4), and MD elongates (Elo-18), but the sites differed in the abundances of each of these. Tracheary elements (Tra-1) and compound spheres (Cl-5) were also less commonly observed (Data Repository 3).

The average percentage of GSSCs was 9.0% ($\sigma = 3.3\%$) with a range of ~7.0–11.0%. The most commonly observed GSSCs included general (CO-1, Type A & B) and truly conical (CO-2) rondels indicative of pooid grasses. Few rondels with concave/convex bases (COF-5) were also observed. The non-plant biosilica percentage for Matador Ranch was the highest of any other site (1.7%; Data Repository 4).

The second set of samples, which yielded >100 diagnostic morphotypes, are rather different than the two higher yielding sites and are here reported as a percentage of total biosilica (i.e., total phytolith population + diatoms + chrysophytes + sponge spicules + unknown). These two samples "sandwich" the high yielding samples stratigraphically. Most of the diagnostic phytoliths in these samples were echinate spheres (Clm-2, palms) and MD elongates (Elo-18). Anticlinal epidermal cells (Epi-3), tracheary elements (Tra-1, Tra-2), multifaceted S-bodies (Scl-2), VI-1 spheres, and a very few small pink spheres (Cl-4) were also observed. Common GSSCs included general conical rondels (CO-1 Types A and B), *Chusquea*-type rondels (CO-3; bambusoid grasses) and a small number of true saddles (SA-1; chloridoid grasses). The two

lower-yielding samples had the highest percentage of biosilica (sponge spicules and diatoms) of any other sample counted in any of the localities (10.2%) (Data Repository 3, 4 and 5). No overall trend was apparent, despite variability among the samples.

4. Discussion

4.1 Comparison with Global EOT Record

In contrast to marine studies, which record a dramatic perturbation in $\delta^{18}O$, our record of continental paleoclimate in southwestern Montana remains relatively steady throughout the EOT (Figure 5). The new results are consistent with previous lower resolution records (Sheldon and Retallack, 2004; Retallack, 2007) from nearby sites. Steady paleotemperatures and paleprecipitation values in Montana may be linked to the sheltered intercontinental local geography. For example, Sheldon et al. (2012) used stable carbon isotopes, whole rock geochemistry, and depth to the Bk horizon to reconstruct paleoclimate in the Ebro Basin (Spain) during the EOT, and also found little or no paleoclimatic change, in spite of a significant decrease in chemical weathering and hydrospheric reorganization consistent with major ice sheet growth during the onset of the Oi-1 glaciation. The new record is consistent with a growing literature that indicates relatively modest continental interior climatic response characterized by minor cooling (e.g., Terry, 2001; Sheldon, 2009), and more significant responses in near-coastal areas (Sheldon and Retallack, 2004; Sheldon et al., 2009) characterized by cooling of comparable magnitude to the marine response (e.g., Liu et al., 2009). This suggests that climatic response is coupled at the regional scale to hydrospheric response to the global drop in pCO_2^{atm} (Sheldon et al., 2012).

4.2 Stable Carbon Isotopes

The range of carbon isotope values observed (-20.31 to -24.90‰) is characteristic of C_3 vegetation. While many studies have used organic (particularly leaf) carbon data to interpret paleoclimate, care must be exercised to include plant functional types (PFT; i.e., deciduous angiosperm, evergreen gymnosperm, etc.) and local precipitation estimates in the interpretation of this data, as these factors influence $\delta^{13}C_{org}$ (Diefendorf et al., 2010). For example, Diefendorf et al.'s (2010) study of woody C_3 vegetation found that physiological differences cause evergreen gymnosperms and deciduous angiosperms to differ consistently in $\delta^{13}C_{org}$ values, even under similar climate conditions. Our $\delta^{13}C_{org}$ observations combined with mean estimates from Eq (1) are most comparable to Diefendorf et al.'s (2010) "cool-cold deciduous forest."

4.3 Vegetation

In total, forty morphotypes were observed among the five sites. The most diverse site was Big Stonerpipe (28 observed morphotypes), followed by North Hough Draw (25), Little Spring Gulch (22), Little Spring Gulch laterals (22), Little Pipestone (16), and Matador Ranch (13). Diversity observed among FI and GSSC morphotypes individually follow this pattern as well. The most commonly observed phytolith morphotypes observed among the five sites were those indicative of a forested landscape, including small pink spheres (Cl-4) and MD elongates (Elo-18). The most commonly observed GSSC morphotype were general truncated conical rondels (Type A; CO-1). Sedge morphotypes were observed at three sites; Little Spring Gulch (including lateral samples), Big Stonerpipe, and Little Pipestone.

Vegetation reconstruction is based on percentages of FI and GSSC morphotypes only (Data Repository 7) and these values will be used here to discuss paleovegetation in sites examined. The overall FI and GSSC means were 78.0% and 22.1%, respectively (Table 5). The FI site means for North Hough Draw (84.1%), Little Spring Gulch (68.7%), Big Stonerpipe

(73.0%), Little Pipestone (73.1%), and Matador Ranch (84.0%), all remained within one standard deviation of the overall average, suggesting a similar amount of closed forest. The GSSC site means for Little Spring Gulch (31.3%), Big Stonerpipe (27.0%), and Little Pipestone (26.9%) all remained within one standard deviation of the overall mean, but the North Hough Draw (15.9%), Little Spring Gulch laterals (15.2%), and Matador Ranch (16.0%) were more than one standard deviation lower (Table 5) suggesting these latter sites had fewer grasses. Overall vegetation appears to be dominated by forests and woodlands, with palms and open habitat grasses playing a comparatively minor role in the ecosystem (Figure 5).

Although no locality displayed a strong intra-site trend with regard to time or lithology (Figure 5), a clear trend is observed in inter-site comparisons of the relative percentage of open-habitat grasses (Figure 6). These open-habitat grasses were the most commonly counted GSSC morphotypes (CO-1 A and B; CO-2) and likely represent pooid grasses, a C_3 grass subfamily that today live in open, cool and wet climates compared to the C_4 grass families, which are better adapted to warmer, more arid conditions (Strömberg, 2005). Assuming correctly inferred locality ages, open-habitat grasses were present in low abundances beginning ~35.3 Ma, peaked around 34.5 Ma, and then declined to pre-peak levels during the Orellan (~33.3 Ma; Figure 5). Corroboration of the C_3 nature of these grasses is supported by our stable carbon isotope data, which falls closely within the carbon signature range for C_3 plants (~-22 to -30 ‰; Diefendorf et al., 2010). Based on the relatively high percentage of FI morphotypes and palms, coupled with the almost exclusive presence of open-habitat pooid grass morphotypes, we interpret vegetation structure to have included a patchy network of forest and woodlands. The relatively limited percent of grass morphotypes (9.0–22.3 %) indicates they may have played a comparatively minor role in ecosystem structure during this time. This is comparable to Diefendorf et al.'s

(2010) $\delta^{13}C_{org}$ data for woody C_3 plants, which predicted a cool-climate deciduous forest biome for the $\delta^{13}C_{org}$ range observed.

Strömberg's (2005) study on phytolith records from the Eocene-Miocene of the Great Plains showed the presence of open-habitat grasses from the EOT in Colorado, but for Montana and Idaho inferred the presence of closed forest habitats with some understory grasses and a low frequency of open-habitat grasses. One issue is that the dominant GSSCs in Montana seem to be of rondels that are not diagnostic of pooids (an observation confirmed by Miller et al. in press and in the current study), so their ecology is difficult to infer (Strömberg, 2005). However, these are likely to be open-habitat grasses that were replaced by other pooid lineages by the Miocene (Miller et al., in press). This interpretation would be consistent with Sheldon and Hamer (2010) , who inferred open habitats in the late Eocene-early Oligocene based on trace fossil assemblages in southwestern Montana, and with open-habitat (*Stipa*) grass macrofossils from the latest Eocene (~34 Ma) in Colorado (Manchester, 2001).

Macrofossil studies from southwestern Montana over the EOT emphasize the presence of mixed coniferous and broad-leaved deciduous forest with shrubland presumably playing a more minor ecosystem role. This is to be expected as monocots such as grasses are not as well preserved (Herendeen and Crane, 1995; Smith et al., 2010). This is especially true for the EOT, when drying conditions and reduced volcanic activity in the Oligocene hampered fossil preservation in the northern Rocky Mountains (Graham, 1999).

The muted vegetation change observed within site samples is expected based on the relatively short time period spanned by each locality (~200 ka–2 Ma years), as well as the recorded pedotypes that likewise are quite homogeneous in regard to length of development and physical features (color, parent material, etc.; Table 1). Geochemical analyses in conjunction

with paleoclimate proxies described above corroborate the unchanging nature of the soils. Further, the small variation observed in the $\delta^{13}C_{org}$ data mirrors the change in open-habitat grass abundance (Figure 7). Mid-Chadronian samples show comparably moderate values, followed by a Late-Chadronian depletion of 1.62‰ (indicative of drier conditions). Latest-Chadronian samples indicate a 2.46‰ enrichment, followed by return to pre-depletion values around -22.00 ‰ (Figure 7; Table 4).

4.4 Conclusions

A broad understanding of biome response to climate change is inadequate to accurately predict the effects of future climate change. To make the most accurate predictions of vegetation response, we need to understand localized responses to global changes and how regional climate and topography impact biotic change. This study examined five sites in southwestern Montana over the EOT using whole-rock geochemical analyses of paleosols, stable carbon isotope data from organic paleosol inclusions and vegetation reconstruction based on phytoliths. In contrast to marine studies, our record of continental paleoclimate in southwestern Montana remains relatively steady throughout the EOT (Figure 5), indicative of a gradual cooling and drying over this period. The new record is corroborated by other studies (e.g., Terry, 2001; Sheldon, 2009) and suggests that climatic response is coupled at the regional scale to hydrospheric response to the global drop in pCO_2^{atm} (Sheldon et al., 2012). Stable carbon isotope observations combined with mean annual precipitation estimates are most comparable to Diefendorf et al.'s (2010) "cool-cold deciduous forest." Phytolith studies indicate a patchy network of forest and woodlands. The relatively limited percent of grass morphotypes (9.0–22.3 %) indicates they may have played a comparatively minor role in ecosystem structure during this time. Though overall vegetation change was muted, the proportion of open-habitat pooid grasses did change with time,

an observation matched by $\delta^{13}C_{org,}$ records. Data presented here suggests open-habitat grasses were present in low abundances beginning ~35.3 Ma, peaked around 34.5 Ma, and then declined to pre-peak levels during the Orellan (~33.3 Ma).

4.5 Future Work

This study aimed to provide a high resolution image of intermontane vegetation during the EOT in Montana. While many paleoclimate studies have relied on far fewer samples than presented in this study, more data is needed to achieve a more continuous record. The small section size of most sampled localities meant that geochemical and phytolith data provide a snapshot covering ~200 ka–2 Ma years. Furthermore, clearer understanding of EOT vegetation change could be achieved via better age-constrained sample localities.

5.0 Acknowledgements

Literature Cited

Becker, H.F., 1960, The Tertiary Mormon Creek Flora from the Upper Ruby River Basin in southwestern Montana, Palaeontographica, v. 107, p. 83-126.

Becker, H.F., 1961, Oligocene plants from the upper Ruby River Basin, southwestern Montana. Geol. Soc.Amer. Mem, v. 82, p. 1-127.

Becker, H.F., 1969, Fossil plants of the Tertiary Beaverhead Basins in southwestern Montana, Palaeontographica, v. 127, p. 1-142.

Becker, H.F., 1972, The Metzel Ranch Flora of the Upper Ruby River Basin, southwestern Montana, Palaeontographica, v. 141, p. 1-61.

Becker, H.F., 1973, The York Ranch Flora of the Upper Ruby River Basin, southwestern Montana, Palaeontographica, v. 143, p. 18-93.

Coxall, H.K., Wilson, P.A., Pälike, H., Lear, C.H., Backman, J., 2005, Rapid stepwise onset of Antarctic glaciations and deeper calcite compensation in the Pacific Ocean: Nature, v. 433, p. 53-56.

DeConto, R.M., Pollard, D., Wilson, P.A., Pälike, H., Lear, C.H., Pagani, M., 2008, Thresholds for Cenozoic bipolar glaciations: Nature, v. 455, p. 652-656.

Diefendorf, A.F., Mueller, K.E., Wing, S.L., Koch, P.L., Freeman, K.H., 2010, Global patterns in leaf 13C discrimination and implications for studies of past and future climate: PNAS, v. 107, p. 5738-5743.

Douglass, E., 1905, The Tertiary of Montana. Mem. Carnegie Museum, v. 2, p. 203-224.

Fields, R.W., Tabrum, A.R., Rasmussen, D.L., Nichols, R., 1985, Cenozoic rocks of the intermontane basins of western Montana and eastern Idaho: A Summary: Cenozoic Paleogeography of West-Central United States, p. 9-30.

Fritz, W.J., Sears, J.W., McDowell, R.J., Wampler, J.M., 2007, Cenozoic Volcanic Rocks of Southwestern Montana: The Journal of the Tobacco Root Geological Society, v. 36, p. 91-110.

Graham, A., 1999, Late Cretaceous and Cenozoic History of North American Vegetation: Oxford University Press, Inc; New York.

Grimes, S.T., Hooker, J.J., Collinson, M.E., Mattey, D.P., 2005, Summer temperatures of late Eocene to early Oligocene freshwaters: Geology, v. 33, p. 189-192.

Herendeen, P. S., and Crane, P. R., 1995, The fossil history of the monocotyledons. p. 1-21 *In* P. J. Rudall, P. J. Cribb, D. F. Cutler, C. J. Humphries [eds.], Monocotyledons: systematics and evolution. Royal Botanic Gardens, Kew, UK.

Hooker, J.J., 1995, Reconstruction of land and freshwater palaeoenvironments near the Eocene-Oligocene boundary, southern England: Journal of the Geological Society, v. 152, p. 449-468.

Hooker, J.J., Grimes, S.T., Mattey, D.P., Collinson, M.E., Sheldon, N.D., 2009, Refined correlation of the UK Late Eocene-Early Oligocene Solent Group and timing of its climate history, The Geological Society of America, Special Paper 452, p. 179-192.

Hutchison, J.H., 1992, Western North America Reptile and Amphibian Record Across the Eocene/Oligocene Boundary and Its Climatic Implications. Pp. 451-463 *n*: Prothero, D.R., Berggren, W.A. (eds.), Eocene-Oligocene Climatic and Biotic Evolution.

Ivany, L.C., Patterson, W.P., Lohmann, K.C., 2000, Cooler winters as a possible cause of mass extinctions at the Eocene/Oligocene boundary: Nature, v. 407, p. 887-890.

Jenny, H.J., 1941, Factors of Soil Formation, McGraw-Hill, New York. 281 pp.

Lear, C.H., Elderfield, H., Wilson, P.A., 2000, Cenozoic Deep-Sea Temperatures and Global Ice Volumes from Mg/Ca in Benthic Foraminiferal Calcite: Science, v. 287, p. 269-272

Liu, Z., Pagani, M., Zinniker, D., DeConto, R., Huber, M., Brinkhuis, H., Shah, S.R., Leckie, R.M., Pearson, A, 2009, Global Cooling During the Eocene-Oligocene Climate Transition: Science, v. 323, p. 1187-1190

Manchester, S.R., 2001, 4. Update on the megafossil flora of Florissant, Colorado. p.137-161 in Evanoff, E., Gregory-Wodzicki, K.M., Johnson, K.R., eds, Fossil Flora and Stratigraphy of the Florissant Formation, Colorado (Denver Museum of Nature and Science, Denver), Series 4, No. 1.

Miller, K.G., Fairbanks, R.G., Mountain, G.S., 1987, Tertiary oxygen isotope synthesis, sea level history, and continental margin erosion: Paleooceanography, v. 2, p. 1-19.

Miller, K.G., Wright, J.D., Browning, J.V., 2005, Visions of ice sheets in a greenhouse world: Marine Geology, v. 217, p. 215-231

Miller, L., Smith, S.Y., Sheldon, N.D., Strömberg, C.A.E.. In press. Eocene vegetation and ecosystem fluctuations inferred from a high-resolution phytolith record: GSA Bulletin.

Nichols, R, and Hanneman, D.L., 2001, Overview of Paleontological Resources on Public Lands in Madison and Beaverhead Counties, Montana. BLM Project Report.

Pearson, P.N., Foster, G.L., Wade, B.S., 2009, Atmospheric carbon dioxide through the Eocene-Oligocene climate transition: Nature, v. 461, p. 1110-1113.

Prothero, D.R., 1994, The Late Eocene-Oligocene Extinctions: Annual Review of Earth Planet Science, v. 22, p. 145-65

Raymo, M.E., and Ruddiman, W.F., 1992, Tectonic forcing of late Cenozoic climate: Nature, v. 359, p. 117-122.

Retallack, G.J., 2001, Soils of the Past: An Introduction to Paleopedology, Second Edition. Blackwell Science Ltd, Malden, USA.

Retallack, G.J., 2007, Cenozoic Paleoclimate on Land in North America: The Journal of Geology, v. 115, p. 271-294.

Sheldon, N.D., Retallack, G.J., Tanaka, S., 2002. Geochemical climofunctions from North American soils and applications to paleosols across the Eocene-Oligocene boundary in Oregon. Journal of Geology, v. 110, p. 687-696.

Sheldon, N.D., Retallack, G.J., 2004, Regional Paleoprecipitation Records from the Late Eocene and Oligocene of North America: The Journal of Geology, v. 112, p. 487-494.

Sheldon, N.D., 2009, Nonmarine records of climatic change across the Eocene-Oligocene transition: Geological Society of America, Special Paper, p. 241-248.

Sheldon, N.D., Tabor, N.J., 2009. Quantitative paleoenvironment and paleoclimatic reconstruction using paleosols. Earth-Science Reviews, v. 95, p. 1-52.

Sheldon, N.D. and Hamer, J.M.M. 2010, Evidence for an Early Sagebrush Ecosystem in the Latest Eocene of Montana. The Journal of Geology, v. 118, p. 434-445.

Sheldon, N.D., Costa, E., Cabrera, L., Garces, M., 2012, Continental climate and weathering response to the Eocene-Oligocene transition: The Journal of Geology, in press.

Smith, S.Y., M.E. Collinson, P.J. Rudall and D.A. Simpson. 2010. The Cretaceous and Paleogene fossil record of Poales: review and current research. Pp. 333-356 *In*: O. Seberg, G. Petersen, A. Barfod, J. I. Davis (eds.), Diversity, Phylogeny, and Evolution in Monocotyledons: Proceedings of the Fourth International Conference on the Comparative Biology of the Monocotyledons & the Fifth International Symposium on Grass Systematics and Evolution.

Soil Survey Staff, 2003, Keys to Soil Taxonomy: Ninth Edition. United States Department of Agriculture National Resources Conservation Service. Pp. 13-193.

Strömberg, C.A.E., 2003. The origin and spread of grass-dominated ecosystems during the Tertiary of North America and how it relates to the evolution of hypsodonty in equids. Ph.D. thesis, Department of Integrative Biology, University of California at Berkeley.

Strömberg, C.A.E., 2004. Using phytolith assemblages to reconstruct the origin and spread of grass-dominated habitats in the great plains of North America during the late Eocene to early Miocene. Palaeogeography, Palaeoclimatology, Palaeoecology, v. 207, p. 239-275.

Strömberg, C.A.E., 2005. Decoupled taxonomic radiation and ecological expansion of open-habitat grasses in the Cenozoic of North America. Proceedings of the National Academy of Sciences of the United States of America, v. 34, p. 11980-11984.

Strömberg, C.A.E., 2007. The spread of grass-dominated habitats in Turkey and surrounding areas during the Cenozoic: Phytolith evidence. Palaeogeography, Palaeoclimatology, Palaeoecology, v. 250, p. 10-49.

Strömberg, C.A.E., 2009. Methodological concerns for analysis of phytolith assemblages: Does count size matter?: Quaternary International, v. 193, p. 124-140.

Squires, R.L., 2003, Turnovers in Marine Gastropod Gaunas During the Eocene-Oligocene Transition, West Coast of the United States: in From Greenhouse to Icehouse, Prothero et al. 2003

Tabrum, A.R., Prothero, D.R., Garcia, D., 1996, Magnetostratigraphy and Biostratigraphy of the Eocene-Oligocene Transition, Southwestern Montana, in Prothero D.R., Emry, R.J., eds., The Terrestrial Eocene-Oligocene Transition in North America: Cambridge University Press, p. 278-311.

Tanai, T., Wolfe, J.A., 1977, Revisions of Ulmus and Zelkova in the Middle and Late Tertiary of Western North America, U.S. Geological Survey, Reston, VA. Professional Paper 1026, p. 1-14.

Terry, D.O., 2001, Paleopedology of the Chadron Formation of Northwestern Nebraska: implications for paleoclimate change in the North American midcontinent across the Eocene-Oligocene boundary: Palaeogeography, Palaeoclimatology, Palaeoecology, v. 168, p. 1-38.

Tiffney, B.H., and Manchester, S.R., 2001, The Use of Geological and Paleontological Evidence in Evaluating Plant Phylogeographic Hypotheses in the Northern Hemisphere Tertiary: International Journal of Plant Science.

Tripati, A.K., Eagle, R.A., Morton, A., Dowdeswell, J.A., Atkinson, K.L., Bahe, Y., Dawber, C.F., Khadun, E., Shaw, R.M.H., Shorttle, O., Thanabalasundaram, L., 2008, Evidence for glaciations in the Northern Hemisphere back to 44 Ma from ice-rafted debris in the Greenland Sea: Earth and Planetary Science Letters, v. 265, p. 112-122.

Zachos, J., Pagani, M., Sloan, L., Thomas, E., and Billups, K., 2001, Trends, rhythms and aberrations in global climate 65 Ma to present: Science, v. 292, p. 686-693.

Zanazzi, A., Kohn, M. J., MacFadden, B.J., Terry, D.O., 2007, Large temperature drop across the Eocene-Oligocene transition in central North America: Nature, v. 445, p. 639-642.

Vinogradov, A.P., 1959, The Geochemistry of Rare and Dispersed Chemical Elements in Soils; Consultants Bureau, Inc.; New York.

Wing, S.L., 1987, Eocene and Oligocene Floras and Vegetation of the Rocky Mountains: Annals of the Missouri Botanical Garden, v. 74, p. 748-784
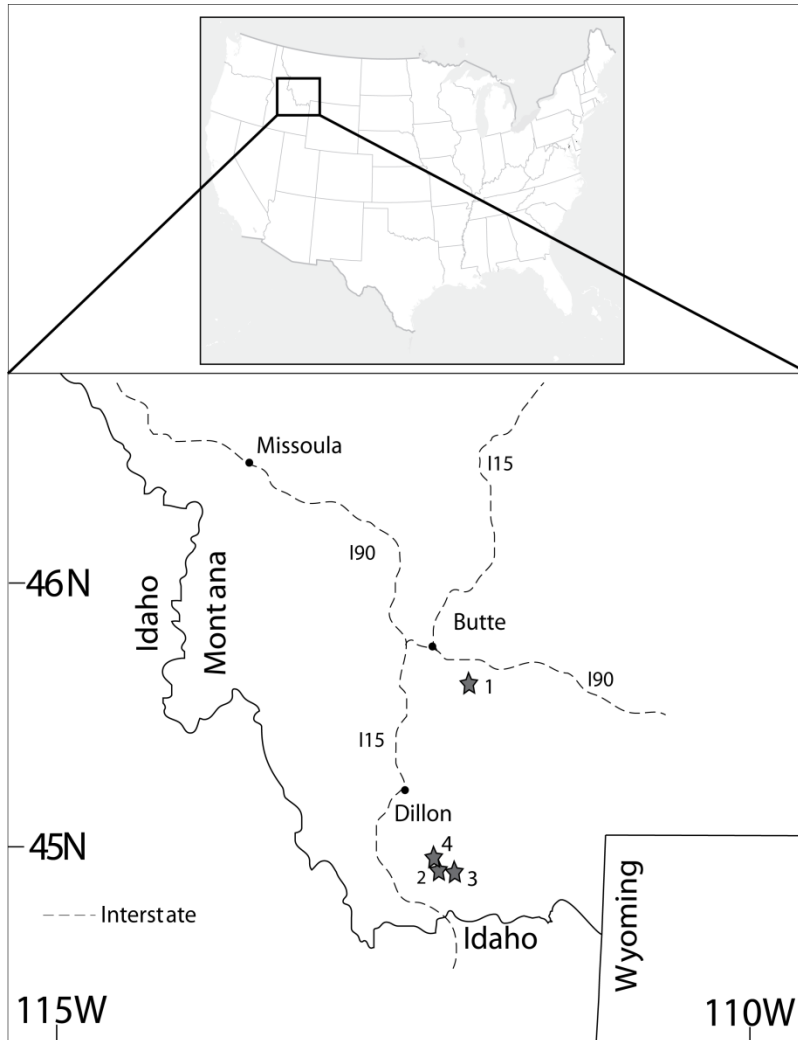
Figure 1. Location of sites in southwest Montana sampled in this study.
Evidence from phytoliths and paleosols are used to create a broad regional record of local vegetation and climate from five biostratigraphically dated sites in southwestern Montana across the EOT: (1) Little Pipestone and Big Stonerpipe (latest Chadronian), (2) North Hough Draw #1 (middle/late Chadronian), (3) Matador Ranch (Orellan), (4) Little Spring Gulch (Chadronian). Site ages based on North American Land Mammal Ages (NALMA).
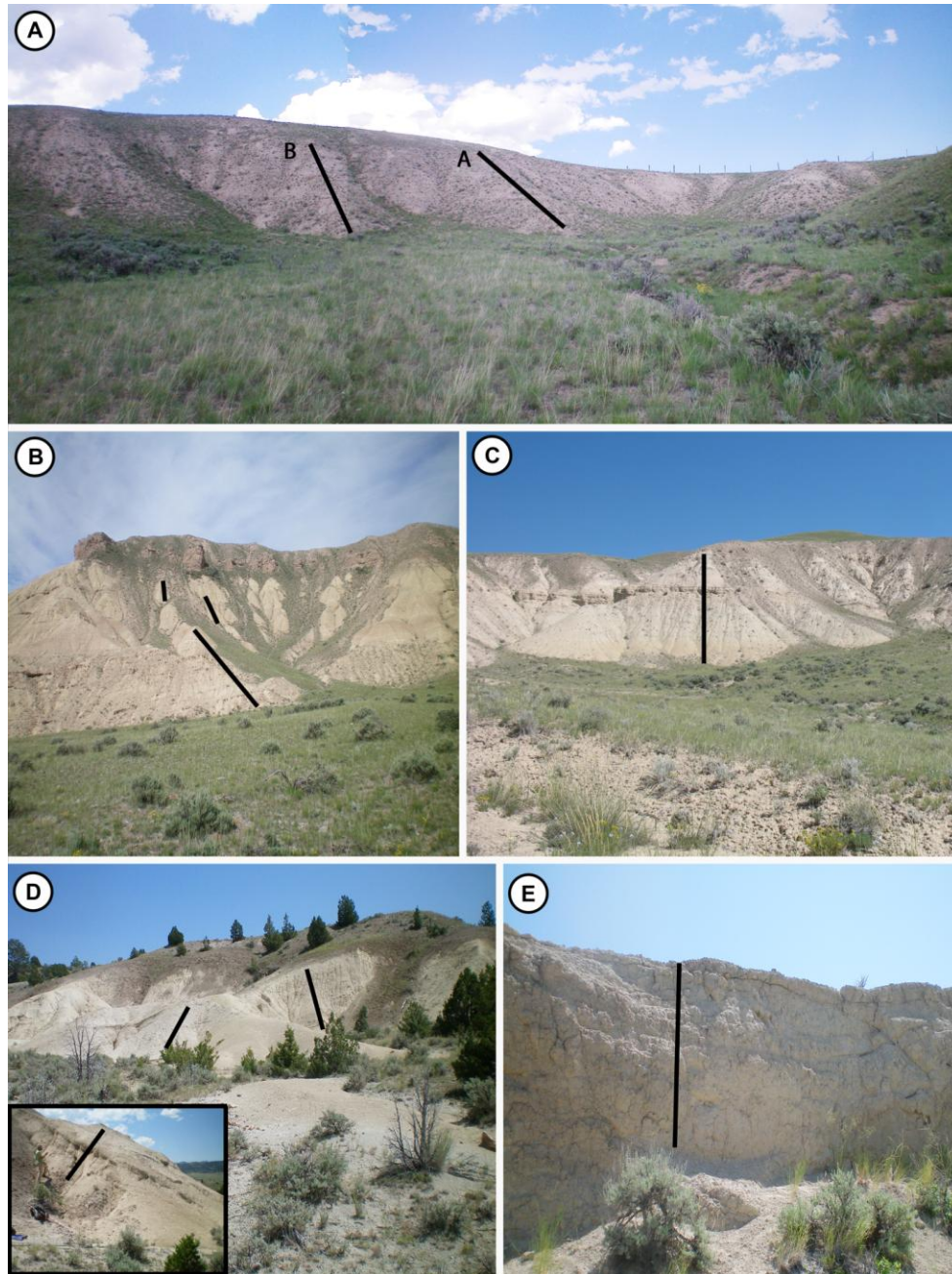
Figure 2. Photographs of the sample localities.
Black lines represent sampled section lines. (A) Little Spring Gulch (N 44° 50' 19.6", W 112° 35' 52.9"). Two sections were sampled to comprise Little Spring Gulch ("A" and "B" on photo). Lateral samples were taken from section between A and B, as well as on outcrop to right of B. Note BLM fence on ridge crest for scale. (B) Matador Ranch (N 44° 45' 1", W 112° 33' 59.7"). Sections were generally correlated by white/light gray ash marker beds. Dark sediment unconformably overlying lighter basal sediment is the Sixmile Creek Formation, while lighter sediment is the Renova Formation. (C) North Hough Draw (N 44° 45' 17.8", W 112° 34' 45.2"). Sampled section taken between ~15 m covered section on top and 8-10 m covered section below. (D) Big Stonerpipe (N 45° 50' 35.7", W 112° 15' 20.5"). Inset photo shows rightmost part of locality. (E) Little Pipestone. See Sheldon and Hamer (2010) for full site description.
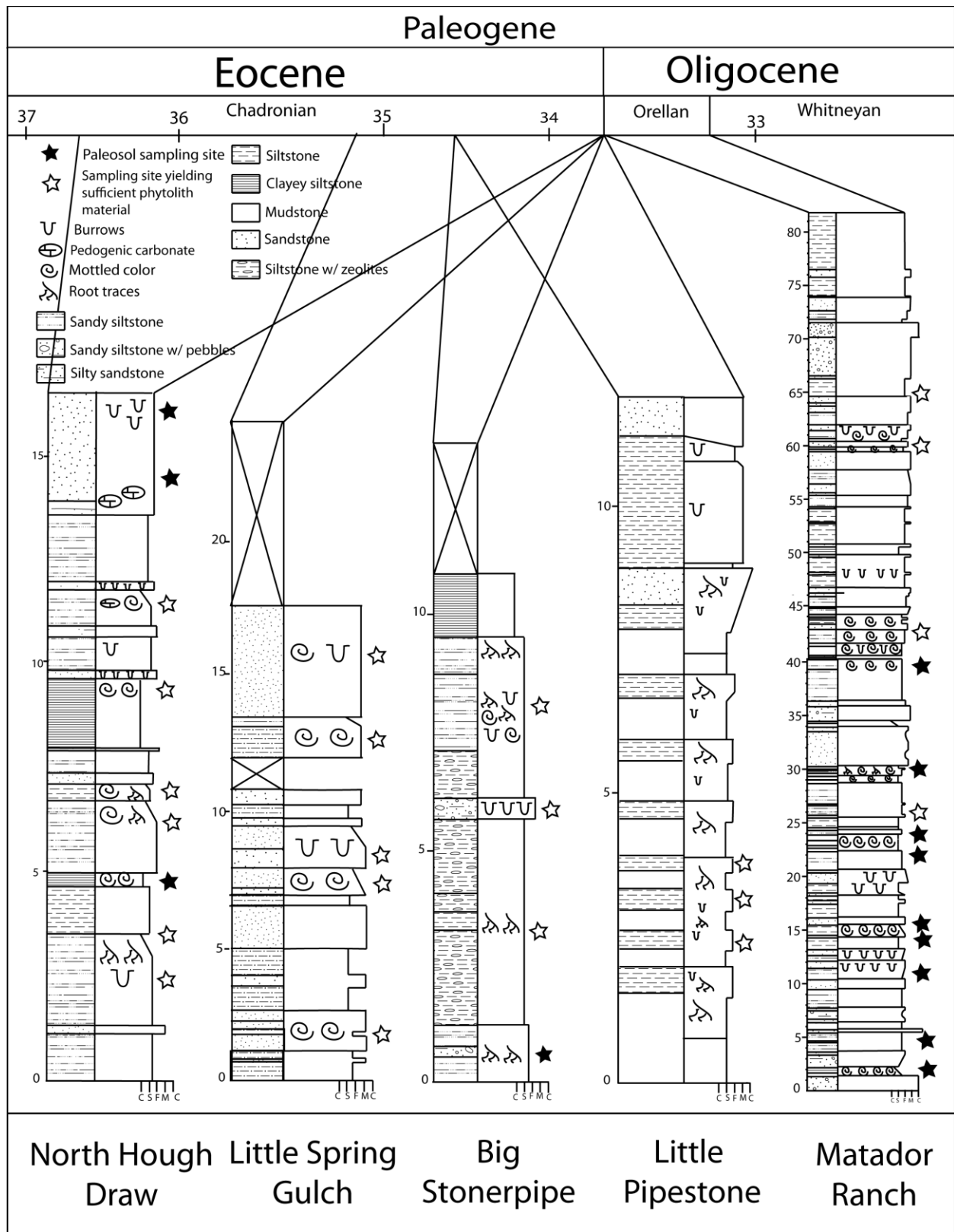
Figure 3. **Stratigraphic logs, ages, and sampling for Renova Basin study sites.**
Grain size indicated: C=clay, S=silt, F=fine sand, M=medium sand, Co=coarse sand).

6
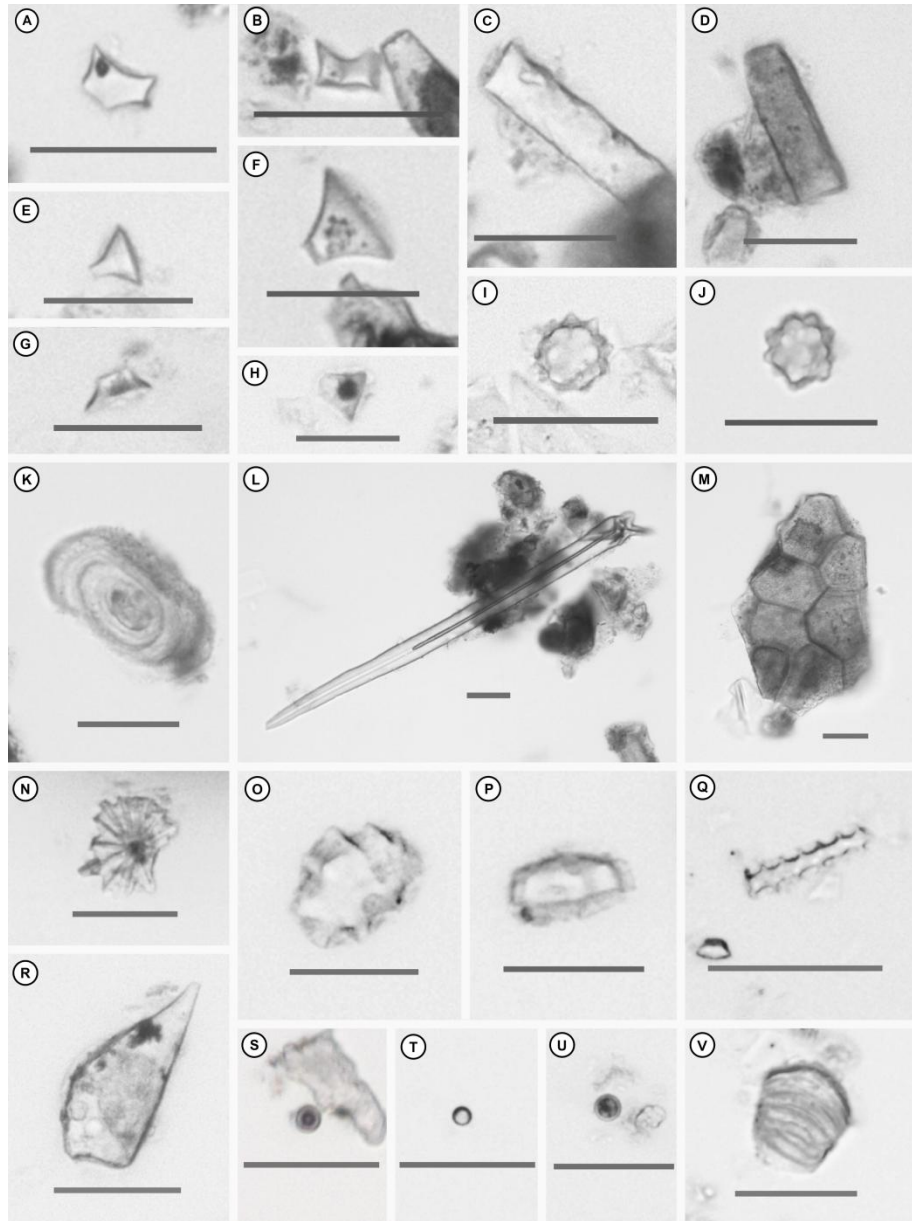
Figure 4. Microphotographs of selected phytolith morphotypes from Renova Basin study sites.
Compound variables indicated in parentheses. (A) CO-4: small "spiked" rondel with concave base in side view and a top equal in size to the base (OTHG; from XXX). (B) SA-3: collapsed saddle (BAMB/B; from Big Stonerpipe). (C) Elo-1: smooth elongates (OTH). This was the dominant morphotype at each locality, but is non-diagnostic so was not used in vegetation reconstruction. (D) Elo-18: MD elongate (DICOT-WO; from Little Spring Gulch). (E-G) CO-1 generic conical rondels (POOID-ND; from Little Spring Gulch). (H) CO-2: truly conical rondel (POOID-D; from Little Spring Gulch). (I, J) Clm-2: echinate sphere (PALM; from Matador Ranch (I) and Little Spring Gulch (J)). (K) VI-1: laminated sphere (DICOT-GEN; from Big Stonerpipe). (L) Sponge spicule, not included in vegetation reconstruction, but used as an indication of proximity to water (Matador Ranch). (M) Unknown phytolith, resembling M-3 (concentric silica aggregate), but lacking organization around a central point. Excluded from analysis. (Matador Ranch). (N) Unknown morphotype. May be abraded aquatic biosilica. (from Little Spring Gulch). (O, P) 3D anticlinal epidermal cells (Epi-3). "Puffy puzzle pieces." Note flat bottom side in (P) (DICOT-GEN; from North Hough Draw). (Q) Tra-1: tracheary element (FI-GEN; from Little Spring Gulch). (R) Tri-8: spindle-shaped body (GRASS/MONO-ND; from Little Spring Gulch). (S,T,U) Cl-4: small pink spheres (FI-GEN; from North Hough Draw (S) and Matador Ranch (T,U)). (V) Tra-2: worm/pupa-like, infilled helical tracheary element (FI-GEN; from Big Stonerpipe). Scale bars = 10 µm.

37
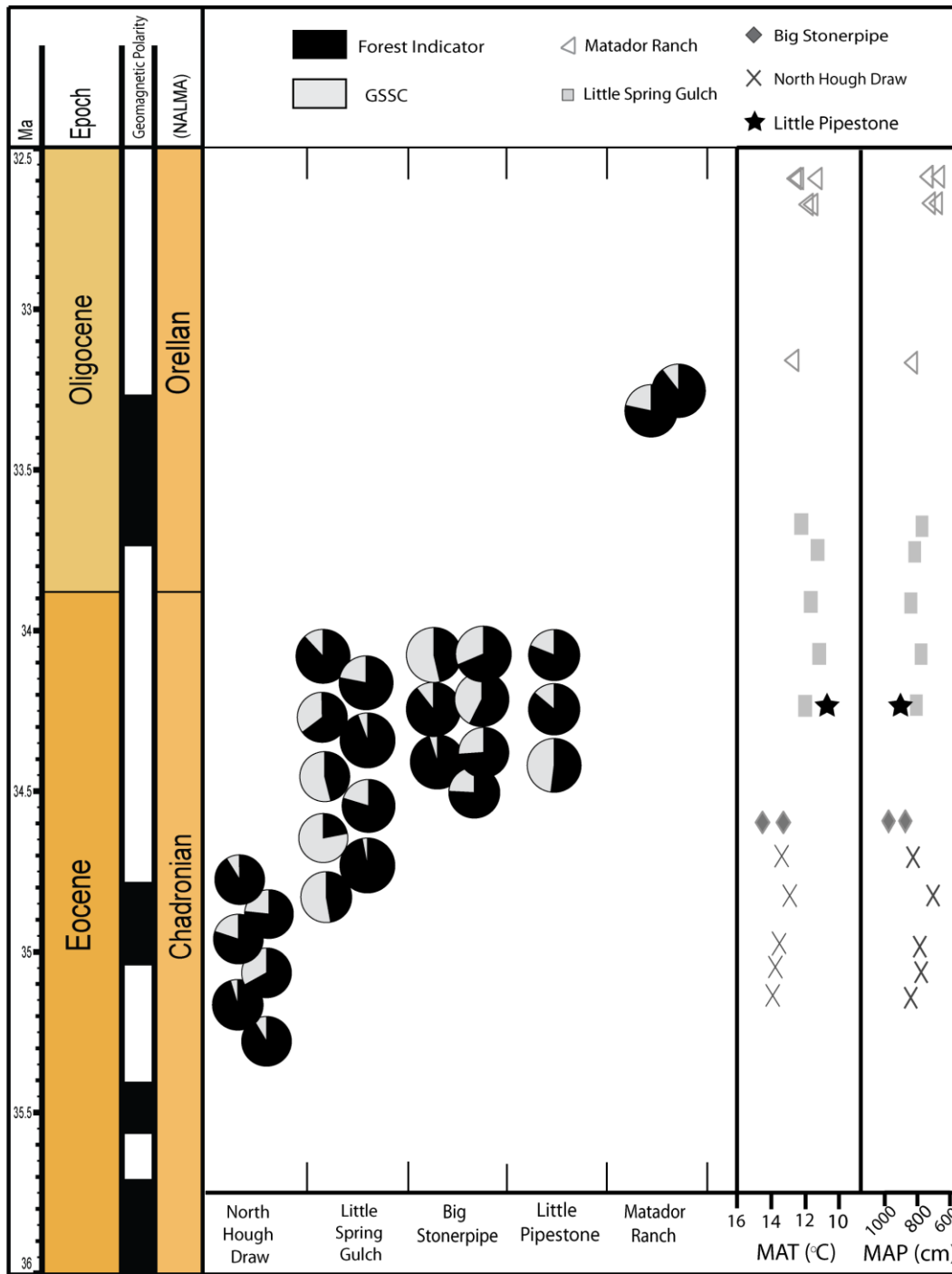
Figure 5. Vegetation reconstruction and paleoclimate for Renova Basin EOT sites.
Inferred paleovegetation shown as pie charts with percent forest indicator (FI; dark) and grass (GSSC; light) inferred from phytolith assemblage analysis. See text for explanation of dating. Geochemical data (on the right) for all five sites provide proxy estimation of mean annual temperature (MAT) and mean annual precipitation (MAP). Both proxies show a slight cooling and drying trend during the Orellan (Matador Ranch samples).
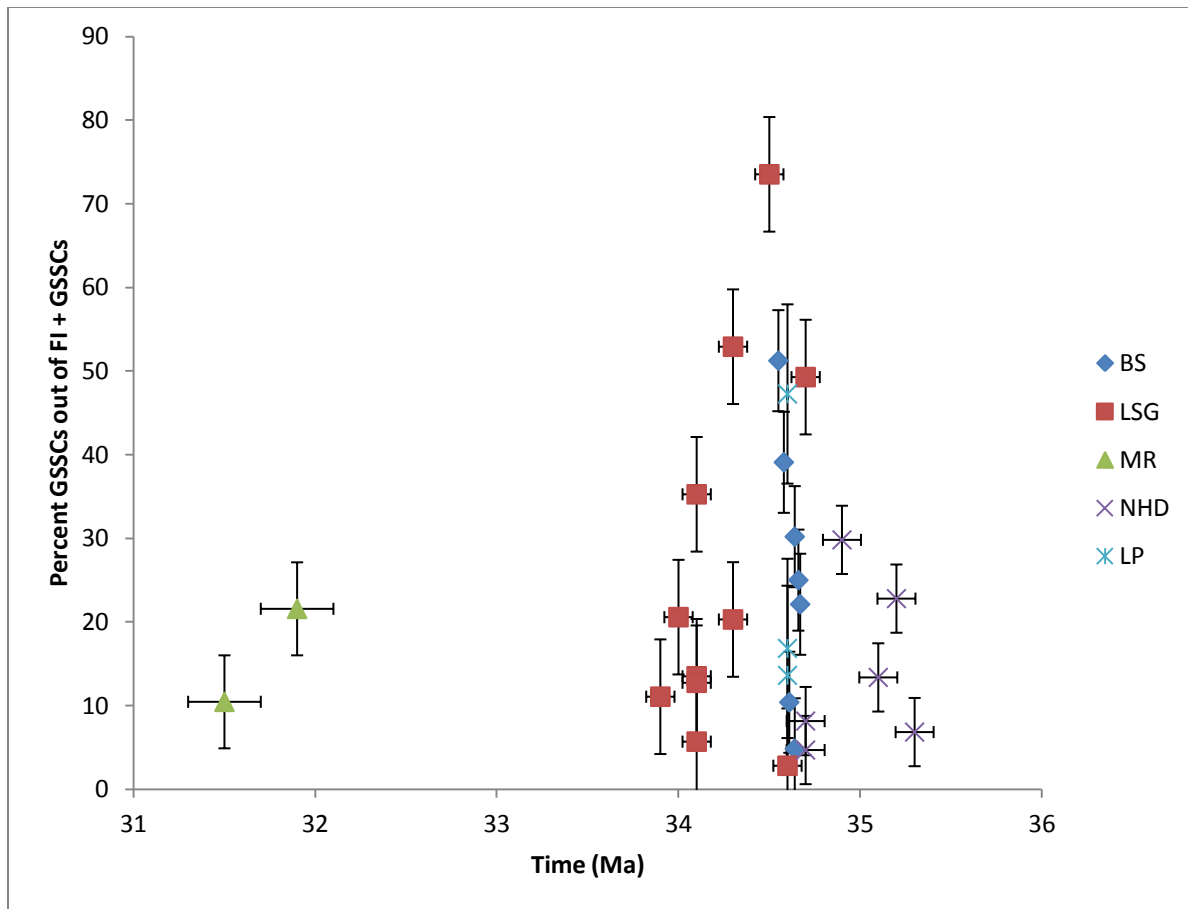
Figure 6. Changes in inferred amounts of open-habitat GSSC morphotypes over time (Ma). BS = Big Stonerpipe, LSG = Little Spring Gulch, MR = Matador Ranch, NHD = North Hough Draw, and LP = Little Pipestone.
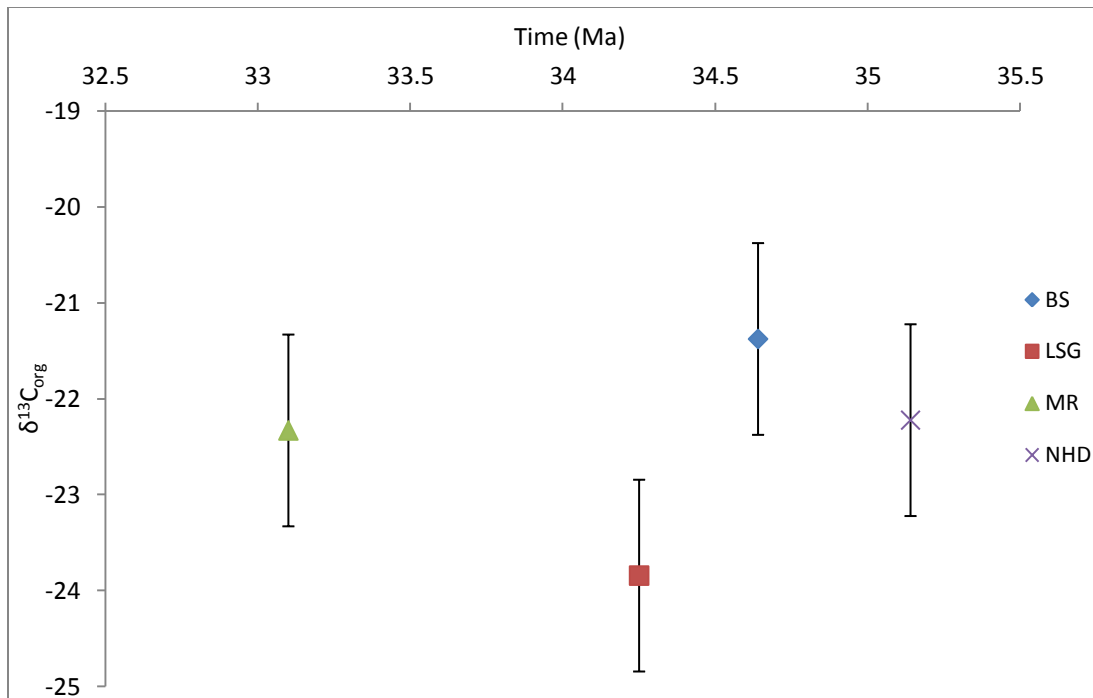
Figure 7. Mean isotope data plotted as $\delta^{13}C_{org}$ against time. BS = Big Stonerpipe, LSG = Little Spring Gulch, MR = Matador Ranch, and NHD = North Hough Draw.

Table 1. Pedotype description and distribution during Eocene-Oligocene Transition, southwestern Montana. ENT = Entisol, INCEP = Inceptisol, RWA = Reworked ash, QP = Quartz pebbles, silt = siltstone, sand = sandstone, (f) = fine, (m) = medium, (m/f) = medium/fine, RT = root traces

Pedotype	Sample #	Meter Level	Soil Order	Horizon	Munsell Color	Parent Material	Depositional Setting	Other Notes
Santo Hoyo	LP-11	4.6	ENT	A	2.5Y 7/2	silt (QP),RWA	distal alluvial fan edges	burrows (Taenidium,)
Santo Hoyo	MR-20	29.3	ENT	A	2.5Y 7/4	sandy silt	floodplain	5 cm above mottled layer
Santo Hoyo	LP-10	3.1	ENT	A	2.5Y 7/2	clayey silt	distal alluvial fan edges	indurated (Taenidium burrows)
Santo Hoyo	LP-05	10.7	ENT	A	2.5Y 6/3	clayey silt	distal alluvial fan edges	burrows
Santo Hoyo	LSGB-07	8.9	ENT	A	10YR 7/2	sand (m/f)	floodplain	burrows
Santo Hoyo	LSGB-12	14.5	ENT	A	10YR 8/1	sand (f)	floodplain	burrows
Santo Hoyo	NHD-10	16	ENT	A	Gley 1 8/1, 2.5Y 8/2	sand (f)	floodplain	Burrows (Taenidium)
Santo Hoyo	LP-02	3.5	ENT	A	2.5Y 6/3	silt w/ rare ash		RT
Santo Hoyo	LP-06	10.7	ENT	A	2.5Y 7/3	RWA, silt (QP)	distal alluvial fan	RT
Santo Hoyo	LSGB-04	4.2	ENT	A	10YR 7/2	silty sand	distal alluvial fan edges	RT
Santo Hoyo	LSGB-05	13.2	ENT	A	10YR 7/2	sily sand (QP)	distal alluvial fan edges	RT
Santo Hoyo	LSGB-11	13.1	ENT	A	10YR 6/3	silty sand	distal alluvial fan edges	RT
Santo Hoyo	NHD-01,02	3.4	ENT	A	2.5Y 7/3	sandy (f) silt	floodplain	RT, rare burrows
Santo Hoyo	LP-07	0.4	ENT	A	2.5Y 7/2	sandy silt (QP)	floodplain	RT
Anegado	NHD-04	6.7	ENT	Bg	2.5Y 7/3	silt	distal alluvial fan edges	RT (drab haloed--grn halos in brn matrix)
Anegado	MR-12	22.4	INCEP	Bg	5Y 8/4, 2.5Y 7/4	sandy silt	floodplain (continuously waterlogged)	gleyed bottom of a Bg horizon
Anegado	MR-13	22.6	INCEP	A/Bg	2.5Y 6/3	Sandy silt	Floodplain (CW)	Gleyed w/ slickensides
Anegado	MR-04,05,06	6.1	INCEP	Bg	2.5Y 6/3	Sandy silt	Floodplain (CW)	Gleyed w/ slickensides, rhizoliths
Anegado	MR-09	15	INCEP	Bg	2.5Y 6/4	silt	distal alluvial fan (CW)	green gley

Table 1. Pedotype description and distribution during Eocene-Oligocene Transition, southwestern Montana, continued.

Pedotype	Sample #	Meter Level	Soil Order	Horizon	Munsell Color	Parent Material	Depositional Setting	Other Notes
Con Color	MR-16	24.3	INCEP	Bw	5Y 8/2, 10YR 7/2	silt	distal alluvial fan edges	MOT (brn w/ rare grn)
Con Color	MR-17	24.4	INCEP	Bw	5Y 8/3, 2.5Y 7/3	silt	distal alluvial fan edges	MOT (brn w/ rare grn)
Con Color	MR-28	59.6	INCEP	A	2.5Y 6/3	silt	distal alluvial fan edges	MOT (brn)
Con Color	MR-03	1.9	INCEP	A	10YR 6/3	sandy (f) silt	floodplain	MOT (brn/grn)
Con Color	MR-23	41.1	INCEP	A	10YR 6/3	clayey silt	distal alluvial fan edges	MOT (brn/grn)
Con Color	NHD-06	6.7	INCEP	Bw	2.5Y 7/3	clayey silt	distal alluvial fan edges	MOT (drab grn)
Con Color	LSG-03	7.7	INCEP	Bw	Gley 1 8/1, 10YR 8/2	sandy silt	floodplain	MOT (grn)
Con Color	LSG-05	13.2	INCEP	Bw	Gley 1 8/1, 10YR 6/3	silt	distal alluvial fan edges	MOT (grn)
Con Color	NHD-03	4.9	INCEP	Bw	2.5Y 7/3	clayey silt	distal alluvial fan edges	MOT (grn)
Con Color	LP-08	2.5	INCEP	Bw	2.5Y 8/2	sandy silt	floodplain	MOT (grn)
Con Color	LP-09	0.4	INCEP	A/ Bw	2.5Y 7/3	clayey silt	distal alluvial fan edges	MOT (grn) and RT
Con Color	LP-04	8.7	INCEP	A	2.5Y 7/3	silt (QP), RWA	distal alluvial fan edges	MOT (grn), burrows
Con Color	MR-02	1.7	INCEP	Bw	5Y 5/2	fine sandy silt	distal alluvial fan edges	MOT (grn/red) (gleyed)
Con Color	MR-15	23.5	INCEP	Bw	2.5Y 7/4	sandy silt	floodplain	MOT (pink w/ grn)
Con Color	LSG-01	1.6	INCEP	Bw	2.5YR 6/2	sandy silt	floodplain	MOT (weak grn)
Con Color	NHD-05	7.1	INCEP	Bw	2.5Y 7/3	sandy (f) silt	floodplain	MOT (weak grn), drab haloed RT
Con Color	LSG-06	15.8	INCEP	A	10YR 6/3	silty sand (f)	distal alluvial fan edges	MOT (weak grn), RT
Con Color	NHD-07,08	11.6	INCEP	Bw	2.5Y 7/3	sandy (f) silt	floodplain	MOT (weak), pedo CO3
Santo Hoyo	LPS-09-01	~2.3	ENT		2.5Y 7/3	ashy silt	floodplain	Burrows (Taenidium)
Santo Hoyo	LPS-09-02	~3.2	ENT		2.5Y 7/3		floodplain	Burrows (Taenidium)
Santo Hoyo	LPS-09-03	~3.9	ENT		2.5Y 7/3	silt	floodplain	Burrows (Taenidium)

Table 2. Raw geochemical data expressed as a percent of total sample.

Sample #	Meter level	Horizon	SiO$_2$	Al$_2$O$_3$	Fe$_2$O$_3$	CaO	MgO	Na$_2$O	K$_2$O	TiO$_2$	MnO
LP11-08	2.5	Bw	58.2	13.45	4.04	2	1.54	1.43	1.45	0.47	0.02
LP11-09	.3	A/Bw	54.5	15.55	5.3	1.83	2.08	1.26	1.03	0.74	0.02
LSG11-03	7.6	Bw	60.3	13.45	4.64	2.57	1.29	1.45	2.37	0.61	0.08
LSG11-04	8.5		66.8	14.21	5.00	2.9	1.32	1.66	3.01	0.63	0.19
LSG11-05	13.2	Bw	60	13.35	4.68	2.32	1.35	1.36	2.67	0.58	0.05
LSG11-06	15.8	A/Bw	61	13.35	5.21	2.42	1.4	1.48	2.84	0.59	0.12
LSGB11-06	6.3	Bw	60.9	13.45	4.45	2.94	2.03	1.43	2.22	0.51	0.15
MR11-02	1.7	Bw	59.4	13.6	5.29	2.36	1.64	1.39	1.88	0.57	0.1
MR11-12	22.4	Bg	61.4	12.05	4.63	3.09	1.55	1.78	1.85	0.54	0.05
MR11-13	22.7	A	60.7	12.05	4.57	3.26	1.41	2.12	1.92	0.55	0.05
MR11-15	23.5	Bg	62.2	12.7	4.93	2.93	1.56	1.66	1.98	0.6	0.05
MR11-16	24.3	Bg	66.8	14.08	5.26	2.9	1.89	2.03	2.40	0.73	0.15
MR11-17	24.4	Bg	59	13.25	5.41	3.9	1.86	1.6	1.79	0.66	0.05
MR11-18	25.4	Bg	57.3	13.9	5.39	3.1	2.04	1.74	1.71	0.56	0.06
MR11-19	25.6	A	57	13.6	5.63	3.02	2.06	1.72	1.57	0.57	0.05
NDH11-03	5	Bg	61.3	14.76	5.96	2.9	2.20	1.80	1.87	0.71	0.48
NDH11-04	6.7		58	13.3	5.15	4.07	1.75	1.68	1.97	0.65	0.05
NDH11-05	7.1	Bg	58.7	13.85	5.04	3.18	1.9	1.69	1.63	0.79	0.03
NDH11-06	9.6	Bg	57.7	13.45	4.73	3.35	1.98	1.46	1.61	0.71	0.04
NDH11-07	11.6		61.1	14.31	5.88	2.9	2.34	1.48	1.66	0.76	0.31

Table 2. Raw geochemical data expressed as a percent of total sample. *LOI = Loss on igntition

Sample #	Meter level	SrO	BaO	LOI	Total	CIA	CIA-K	BaO/SrO	TiO/Al$_2$O$_3$	MAP (mm yr^{-1})	MAT (^{o}C)
LP11-08	2.5	0.03	0.03	18.7	101.5	64.023	69.192	0.676	0.045	863.718	13.239
LP11-09	.3	0.04	0.03	19	101.5	70.474	74.225	0.507	0.061	953.737	14.476
LSG11-03	7.6	0.03	0.06	12.75	99.7	58.293	65.585	1.352	0.058	804.466	11.946
LSG11-04	8.5	0.04	0.11	5.72	99	55.780	63.971	2.027	0.057	779.304	11.116
LSG11-05	13.2	0.02	0.06	12.8	99.3	58.823	67.406	2.027	0.055	833.860	11.615
LSG11-06	15.8	0.02	0.06	10.7	99.3	57.398	66.140	2.027	0.056	813.314	11.213
LSGB11-06	6.3	0.02	0.06	11.4	100	57.111	63.600	2.027	0.048	773.627	12.180
MR11-02	1.7	0.02	0.05	12.15	98.6	61.227	67.402	1.689	0.053	833.794	12.752
MR11-12	22.4	0.03	0.05	12.9	100	53.322	58.506	1.126	0.057	699.756	11.627
MR11-13	22.7	0.04	0.05	13.6	100.5	51.184	56.139	0.845	0.058	667.876	10.998
MR11-15	23.5	0.03	0.06	11.1	100	55.456	61.182	1.352	0.060	737.629	11.898
MR11-16	24.3	0.05	0.08	7.11	101	55.656	62.022	1.126	0.066	749.942	11.374
MR11-17	24.4	0.03	0.05	12.95	101	53.191	57.677	1.126	0.064	688.421	12.467
MR11-18	25.4	0.03	0.06	15	101	57.321	62.058	1.352	0.051	750.468	12.608
MR11-19	25.6	0.03	0.05	15.5	101	57.579	62.043	1.126	0.053	750.256	12.725
NDH11-03	5	0.04	0.06	10.48	99.9	59.014	64.204	0.901	0.062	782.887	12.606
NDH11-04	6.7	0.03	0.13	13.5	100.5	51.962	56.684	2.928	0.062	675.084	12.123
NDH11-05	7.1	0.04	0.05	13.35	100.5	57.288	61.798	0.845	0.073	746.640	12.765
NDH11-06	9.6	0.04	0.05	15.2	100.5	56.787	61.297	0.845	0.067	739.303	12.977
NDH11-07	11.6	0.03	0.07	12.76	101	60.083	64.997	1.689	0.068	795.208	13.135

Table 3. Stable Carbon Isotope Data, expressed relative to VPDB.

Sample #	∂13C, VPDB	Carbon Weight (%)
LP11-02	-22.6428	0.051
LP11-04	-20.3066	0.055
LP11-06	-21.2593	0.047
LP11-07	-21.3673	0.045
LP11-09	-21.3065	0.064
LSG11-06	-22.9499	0.031
LSGB11-04	-23.4142	0.037
LSGB11-05	-22.7675	0.032
LSGB11-11	-24.6635	0.043
LSGB11-L1-01	-24.9004	0.039
LSGB11-L1-03	-23.0652	0.035
LSGB11-L1-04	-24.0671	0.036
LSGB-L1-05	-23.3859	0.039
LSGB-L2-01	-24.5702	0.039
LSGB-L2-02	-24.6604	0.051
MR11-06	-22.3305	0.053
NHD11-01	-21.7215	0.032
NHD11-08	-23.6563	0.033
NHD11-08	-24.0755	0.032
NHD11-09	-20.904	0.019
NHD11-09	-20.7573	0.018

Table 4. Range, mean, and standard deviation values for organic stable carbon isotope data. Sites arranged chronologically younging upward from bottom. *N = 1, no statistics available.

Site	$\delta^{13}C_{org}$ Range (‰)	$\delta^{13}C_{org}$ Mean (‰)	$\delta^{13}C_{org}$ Std. Dev. (‰)
Matador Ranch*	-	-22.33	-
Big Stonerpipe	-22.64 to -20.31	-21.38	0.83
Little Spring Gulch	-24.90 to -22.95	-23.84	0.82
North Hough Draw	-24.08 to -20.76	-22.22	1.55

Table 5. Mean values and standard deviation for phytolith data. Sites arranged chronologically from youngest to oldest. %PP = Percent of phytolith population, %VR = percents used in vegetation reconstruction.

Site	Mean FI (%PP)	Σ FI (%PP)	Mean GSSC (PP)	Σ GSSC (%PP)	Mean FI (%VR)	Σ FI (%VR)	Mean GSSC (%VR)	Σ GSSC (%VR)
MR	49.1	11.1	9.0	3.3	84.0	11.1	16.0	5.5
LP	52.2	25.4	16.1	5.9	73.1	25.4	26.9	9.6
BS	40.5	19.2	12.7	6.5	73.0	19.2	27.0	7.9
LSG	42.5	15.3	20.2	17.6	68.7	15.3	31.3	15.4
LSG lat	62.5	2.4	22.3	1.0	84.8	2.4	15.2	5.2
NHD	54.4	18.9	9.2	5.1	84.1	18.9	15.9	5.5
All sites	50.2	15.4	14.9	6.6	78.0	15.4	22.1	8.2

Data Repository 1. Phytolith morphotype descriptions and corresponding compound variables and vegetation categories used (for definitions, see Strömberg, 2003). FI = forest indicator; GSSC = grass silica short cell. FIs and GSSCs were used for vegetation reconstruction.

Morphotype	Description	Compound variable	Vegetation Category
Epi-3	3D anticlinal epidermis with rounded bumps	DICOT-GEN	FI
Epi-6	Epidermal plate of sedges	SEDGE	Sedge
EpiF-1	Epidermal amoeba body	DICOT-GEN	FI
Tra-1	Hollow and infilled helix	FI-GEN	FI
Tra-2	Worm/pupa like infilled helical tracheary element	FI-GEN	FI
Tra-7	*Podocarpus*-type tracheary element	CONI	FI
Tra-8	Pitted rod tracheary element (monocot-type)	GRASS/MONO-ND	Potential grass
Tri-8	Trichome filling	GRASS/MONO-ND	Potential grass
Clm-2a	Echinate (spiky) sphere	PALM-D	FI, Palm
Cl-4	Small, smooth, pink sphere	FI-GEN	FI
Cl-5	Compound sphere	FI-GEN	FI
VI-1	VI sphere	DICOT-GEN	FI
Elo-1	Smooth elongate	OTH	Other
Elo-3	Faceted elongate	CONI/MONO	Potential grass
Elo-5	Thin, straight, flat band	OTH	Other
Elo-7	Smooth cylindrical elongate	OTH	Other
Elo-11	Rod with knobs	OTH	Other
Elo-18	MD-elongate	DICOT-WO	FI
Elo-20	One sinuate edge elongate	CONI	FI
EloF-2	Smooth elongate w/ faceted edge	OTH	Other
EloF-3	Smooth elongate w/ faceted edge	OTH	Other
Scl-3	Mutifaceted S-body	DICOT-WO?	FI
Scl-2B	Short Scl-1	FI-GEN	FI
Scl-12	Glass shard body	OTH	Other
Blo-3	Faceted rectangular plate	CONI	FI
Blo-7	Thick trapezoidal rectangle with knobs	DICOT-GEN	FI
Kn-9	Irregular body with branched processes	OTH	Other
CO-1 A	Generic (truncated) conical rondel type A	POOID-ND	GSSC
CO-1 B	Generic (truncated) conical rondel type B	POOID-ND	GSSC
CO-2	Truly conical rondel	POOID-D	GSSC
CO-3	*Chusquea* rondel with "spiked" top	BAMB/B	GSSC
CO-4	Small "spiked" rondel	OTHG	Other GSSC
CO-5	Crescentic conical rondel	CHLOR	GSSC
COF-1B	Tall rondel with spiked top	BAMB/B	GSSC
COF-5	Conical rondel with concave/vex base	POOID-ND	GSSC
COF-6	Tall conical rondel with concave plate	BAMB/B	GSSC
KR-1	Regular keeled rondel	POOID-ND	GSSC
Py-2	Almost keel-like small irregular pyramid	BAMB/B	GSSC

Data repository 1, continued.

Morphotype	Description	Compound variable	Vegetation Category
SAF-1	Long pseudo-saddle	CHLOR	GSSC
SA-1	True saddle	CHLOR	GSSC
SA-3	Collapsed saddle	BAMB/B	GSSC
SA-5	Saddle with one indented side	CHLOR	GSSC
Bl-13	Shovel bilobate with rectangular top	BAMB/B	GSSC

Data Repository 2. Definition of compound variables used in phytolith analysis (Strömberg, 2003).

Morphotype group	Plant type group (Compound variable)	Plant type inferred
Non-GSSC	DICOT-WO	Woody dicotyledon
	DICOT-GEN	General (woody or herbaceous) dicotyledon
	FI-GEN	General forest indicator (dicotyledon; conifer/gymnosperms, Marantaceae, fern, to some degree palm, *Selaginella*)
	CONI	Conifer
	CONI-MONO	Conifer/monocotyledon
	PALM-D	Diagnostic palm; forms exclusive to palms
	SEDGE	Sedge
	GRASS/MONO-ND	Grass/monocotyledon; forms abundantly but not exclusively produced in grasses and some other monocotyledons
	GRASS-D	Diagnostic non-GSSC grass; forms exclusively produced in grasses but not used in vegetation analysis
	OTH	Other non-grass plants; nondiagnostic or unknown
GSSC	BAMB/B	"Bambusoid"/basal grasses
	POOID-D	Diagnostic pooid; forms that are highly diagnostic of pooids
	POOID-ND	Nondiagnostic pooid; forms abundantly but not exclusively produced in pooid grasses
	CHLOR	Diagnostic chloridoid; forms that are highly diagnostic of chloridoids
	OTHG	Other GSSC; nondiagnostic or unknown GSSC

Data Repository 3. Soil characteristics and biosilica morphotypes for samples from the Middle Chadronian-Orellan, Sage Creek Basin, Montana. *p = present but not part of count. Sample numbers are based on locality, with LP=Big Stonerpipe, LSG/LSGB=Little Spring Gulch, MR=Matador Ranch, NHD=North Hough Draw, LPS=Little Pipestone.

Sample number	Meter level	Soil type	Soil horizon	Munsell color	Phytolith abundance	Phytolith morphotype (compound variable) Epi-3 (DICOT-GEN)
LP11-02	3.5	Entisol		2.5 Y 7/2	high	0
LP11-03	5.8	Entisol		2.5 Y 7/3	medium	0
LP11-04	8.7	Inceptisol	Bg	2.5 Y 7/3	high	0
LP11-05	10.7	Entisol	Bg	2.5 Y 6/3	medium	0
LP11-06	0.4	Entisol		2.5 Y 7/3	medium	0
LP11-08	2.5	Inceptisol	Bg	2.5 Y 8/2	medium	3
LP11-10	3.1	Entisol		2.5 Y 7/2	medium	0
LSG11-01	1.6	Inceptisol	Bg	2.5 YR 6/2	high	5
LSG11-03	7.7	Inceptisol	Bg	10 YR 8/2, Gley 1 8/1	high	0
LSG11-04	8.5	Entisol		2.5 Y 8/1	medium	0
LSG11-05	13.2	Inceptisol	Bg	10 YR 6/3, Gley 1 8/1	med-high	1
LSG11-06	15.8	Inceptisol	Bg	10 YR 6/3	medium	8
LSGB11-04	4.2	Entisol		10 YR 7/2	high	2
LSGB11-07	8.9	Entisol		10 YR 7/2	medium	10
LSGB11-11	13.1	Entisol		10 YR 6/3	high	7
LSGB11-12	14.5	Entisol		10 YR 8/1	medium	27
MR11-07	9.3	Inceptisol		2.5 Y 6/4	very low	/
MR11-16	24.3	Inceptisol	Bg	5 Y 8/2, 10 YR 7/2	medium	p
MR11-23	41.1	Inceptisol	A	10 YR 6/3	med-low	/
MR11-25	43.7	Inceptisol		2.5 Y 6/3	medium	0
MR11-28	59.6	Inceptisol	A	2.5 Y 6/3	med-low	0
MR11-29	65.3	Inceptisol		2.5 Y 6/3	med-low	p
NHD11-01	3.5	Entisol	Bg	2.5 Y 7/3	med-low	201
NHD11-02	3.3	Entisol	Bg	2.5 Y 7/3	high	181
NHD11-04	6.7	Entisol		2.5 Y 7/3	high	100
NHD11-05	7.1	Inceptisol	Bg	2.5 Y 7/3	medium	87
NHD11-06	6.7	Inceptisol	Bg	2.5 Y 7/3	high	71
NHD11-07	11.6	Inceptisol		2.5 Y 7/3	medium	28
LPS-09-01	~2.3	Entisol		2.5 Y 7/3	high	3
LPS-09-02	~3.2	Entisol		2.5 Y 7/3	high	2
LPS-09-03	~3.9	Entisol		2.5 Y 7/3	high	4
LSGB11-L1-02	~13.7	Entisol		10 YR 6/3	high	9
LSGB11-L1-06	~13.7	Entisol		10 YR 6/3	high	9

Data Repository 3, continued.

Sample number	Phytolith morphotype (compound variable)					
	Epi-6 (SED GE)	Tra-1 (FI-GEN)	Tra-2 (FI-GEN)	Tra-7 (CONI)	Tra-8 (GRASS-MONO-ND)	Tri-8 (GRASS/M ONO-ND)
LP11-02	0	5	0	0	0	0
LP11-03	0	2	0	0	0	0
LP11-04	0	17	1	0	0	0
LP11-05	0	15	2	0	0	0
LP11-06	1	10	0	0	0	0
LP11-08	0	8	0	0	0	0
LP11-10	0	6	1	0	0	0
LSG11-01	0	15	0	0	1	0
LSG11-03	1	4	0	0	7	0
LSG11-04	0	5	0	0	0	0
LSG11-05	0	3	0	0	0	0
LSG11-06	0	6	0	0	0	0
LSGB11-04	0	2	0	0	0	0
LSGB11-07	0	1	0	0	0	0
LSGB11-11	0	9	0	0	0	0
LSGB11-12	0	6	0	0	0	0
MR11-07	/	p	/	/	p	/
MR11-16	/	p	p	/	/	/
MR11-23	/	/	p	/	/	/
MR11-25	0	11	0	0	0	0
MR11-28	0	2	0	0	0	0
MR11-29	/	p	p	/	/	/
NHD11-01	0	0	0	0	0	0
NHD11-02	0	0	0	0	0	0
NHD11-04	0	0	0	7	0	0
NHD11-05	0	7	0	0	0	3
NHD11-06	0	8	0	1	0	0
NHD11-07	0	0	0	0	0	0
LPS-09-01	0	6	0	0	0	0
LPS-09-2	0	2	0	0	0	0
LPS-09-03	3	5	0	0	0	0
LSGB11-L1-02	0	4	0	0	0	0
LSGB11-L1-06	0	5	0	0	0	0

Data Repository 3, continued.

Sample number	Phytolith morphotype (compound variable)					
	Clm-2a (PALM-D)	Cl-4 (FI-GEN)	Cl-5 (FI-GEN)	VI-1 (DICOT-GEN)	Elo-1 (OTH)	Elo-3 (CONI/MONO)
LP11-02	0	176	0	1	92	0
LP11-03	6	155	0	5	55	0
LP11-04	28	17	0	13	80	0
LP11-05	17	3	0	4	326	0
LP11-06	17	80	0	19	312	0
LP11-08	16	91	0	19	162	0
LP11-10	14	102	1	7	205	0
LSG11-01	8	11	0	0	74	0
LSG11-03	8	1	0	2	66	0
LSG11-04	1	56	0	0	117	0
LSG11-05	6	46	0	1	169	0
LSG11-06	18	47	0	49	173	0
LSGB11-04	76	0	0	56	68	0
LSGB11-07	16	81	0	4	80	0
LSGB11-11	27	15	0	75	95	0
LSGB11-12	19	49	0	20	42	2
MR11-07	/	/	/	/	p	/
MR11-16	p	p	/	p	p	/
MR11-23	p	/	/	/	p	/
MR11-25	32	86	1	12	155	0
MR11-28	8	158	0	0	70	0
MR11-29	/	/	/	p	p	/
NHD11-01	3	0	0	0	39	0
NHD11-02	7	5	0	0	28	0
NHD11-04	6	17	0	0	155	0
NHD11-05	6	32	0	4	150	10
NHD11-06	4	14	0	0	207	0
NHD11-07	132	5	0	4	177	2
LPS-09-01	6	85	0	1	208	0
LPS-09-2	10	162	0	5	15	0
LPS-09-03	11	136	0	3	64	0
LSGB11-L1-02	17	83	0	42	48	0
LSGB11-L1-06	13	58	3	60	50	7

Data Repository 3, continued.

Sample number	Phytolith morphotype (compound variable)					
	Elo-5 (OTH)	Elo-11 (OTH)	Elo-17 (OTH)	Elo-18 (DICOT-WO)	Elo-20 (CONI)	EloF-2 (OTH)
LP11-02	0	0	0	15	0	0
LP11-03	0	0	0	13	0	0
LP11-04	0	0	0	54	1	0
LP11-05	0	0	0	35	12	0
LP11-06	0	0	0	27	0	0
LP11-08	0	1	0	20	0	0
LP11-10	0	1	0	8	0	1
LSG11-01	0	0	0	61	0	0
LSG11-03	0	0	0	30	0	0
LSG11-04	0	5	0	39	0	0
LSG11-05	0	0	0	77	0	0
LSG11-06	0	0	0	63	0	0
LSGB11-04	0	0	1	71	0	0
LSGB11-07	0	0	0	49	0	0
LSGB11-11	0	0	0	65	0	0
LSGB11-12	0	1	1	41	0	0
MR11-07	/	/	/	/	/	/
MR11-16	/	/	/	p	/	/
MR11-23	/	/	/	/	/	/
MR11-25	0	0	0	18	0	0
MR11-28	0	0	0	12	0	0
MR11-29	/	/	/	p	/	/
NHD11-01	0	0	0	77	0	0
NHD11-02	1	0	0	0	0	0
NHD11-04	0	0	0	16	0	0
NHD11-05	0	18	0	26	0	0
NHD11-06	0	0	0	47	2	0
NHD11-07	0	9	0	18	0	0
LPS-09-01	0	5	0	4	0	0
LPS-09-2	0	0	0	1	0	0
LPS-09-03	0	0	0	0	0	0
LSGB11-L1-02	0	0	0	10	7	0
LSGB11-L1-06	0	3	0	8	1	0

Data Repository 3, continued.

Sample number	Phytolith morphotype (compound variable)					
	EloF-3 (OTH)	Scl-3 (DICOT-WO?)	Scl-2 B (FI-GEN)	Scl-12 (OTH)	Blo-3 (CONI)	Blo-7 (DICOT-GEN)
LP11-02	0	0	0	0	0	0
LP11-03	4	0	0	0	0	0
LP11-04	0	2	0	0	0	1
LP11-05	0	0	0	0	0	6
LP11-06	6	0	0	0	5	0
LP11-08	1	0	0	0	0	0
LP11-10	1	0	0	0	0	0
LSG11-01	0	0	0	0	0	5
LSG11-03	0	1	0	0	0	0
LSG11-04	0	0	0	0	0	0
LSG11-05	0	0	0	0	0	0
LSG11-06	0	0	0	0	0	0
LSGB11-04	0	0	0	0	0	0
LSGB11-07	0	0	0	0	0	0
LSGB11-11	0	0	0	0	0	0
LSGB11-12	0	0	0	0	0	0
MR11-07	/	/	/	/	/	/
MR11-16	/	p	/	p	/	/
MR11-23	/	/	/	/	/	/
MR11-25	5	0	0	17	0	0
MR11-28	0	0	0	0	0	0
MR11-29	/	/	/	/	/	/
NHD11-01	0	0	0	0	0	4
NHD11-02	0	0	0	0	2	7
NHD11-04	0	0	0	0	0	6
NHD11-05	0	0	0	0	0	0
NHD11-06	0	0	0	0	0	18
NHD11-07	0	0	0	0	0	0
LPS-09-01	0	0	0	0	0	0
LPS-09-2	0	1	0	0	0	0
LPS-09-03	0	0	0	0	0	0
LSGB11-L1-02	0	0	0	0	0	0
LSGB11-L1-06	0	1	13	0	0	0

Data Repository 3, continued.

Sample number	Phytolith morphotype (compound variable)					
	KN-9 (OTH)	CO-1 A (POOID-ND)	CO-1 B (POOID-ND)	CO-2 (POOID-D)	CO-3 (BAMB/B)	CO-4 (OTHG)
LP11-02	0	6	0	4	0	0
LP11-03	0	13	0	6	0	0
LP11-04	0	58	11	0	0	0
LP11-05	0	85	6	4	0	3
LP11-06	0	22	1	13	4	0
LP11-08	0	39	4	0	0	0
LP11-10	0	37	8	6	2	0
LSG11-01	0	78	15	10	0	0
LSG11-03	0	128	11	10	0	1
LSG11-04	0	77	25	11	0	4
LSG11-05	0	41	19	13	0	0
LSG11-06	0	18	4	2	1	0
LSGB11-04	0	5	0	1	0	1
LSGB11-07	0	31	6	4	0	0
LSGB11-11	0	9	2	0	0	1
LSGB11-12	0	25	5	6	0	2
MR11-07	/	/	/	/	/	/
MR11-16	/	p	p	/	p	/
MR11-23	/	/	/	/	/	/
MR11-25	0	28	11	0	0	0
MR11-28	0	15	2	4	0	0
MR11-29	/	p	/	/	/	/
NHD11-01	1	7	5	0	0	0
NHD11-02	0	16	0	1	0	0
NHD11-04	0	44	3	10	0	0
NHD11-05	0	17	6	2	0	0
NHD11-06	1	38	6	4	0	0
NHD11-07	0	8	0	0	0	0
LPS-09-01	0	68	12	7	0	1
LPS-09-2	0	19	2	3	0	1
LPS-09-03	0	17	8	1	0	4
LSGB11-L1-02	0	12	5	0	0	0
LSGB11-L1-06	0	10	1	6	0	0

Data Repository 3, continued.

Sample number	Phytolith morphotype (compound variable)					
	CO-5 (CHLOR)	COF-1 (BAMB/B)	COF-5 (POOID-ND)	COF-6 (BAMB/B)	KR-1 (POOID-ND)	PY-2 (BAMB/B)
LP11-02	0	0	0	0	0	0
LP11-03	0	0	0	0	0	0
LP11-04	0	0	0	0	0	0
LP11-05	0	0	0	0	0	0
LP11-06	0	0	0	0	3	0
LP11-08	0	1	0	1	3	0
LP11-10	0	0	0	0	1	0
LSG11-01	0	0	0	0	0	0
LSG11-03	0	0	0	0	0	0
LSG11-04	0	0	0	0	5	0
LSG11-05	0	0	0	0	0	0
LSG11-06	0	0	0	0	0	1
LSGB11-04	0	0	0	0	0	0
LSGB11-07	0	0	0	0	0	0
LSGB11-11	0	0	0	0	1	0
LSGB11-12	0	0	0	0	7	0
MR11-07	/	/	/	/	/	/
MR11-16	/	/	/	/	/	/
MR11-23	/	/	/	/	/	/
MR11-25	0	0	5	0	0	0
MR11-28	0	0	0	0	0	0
MR11-29	/	/	/	/	/	/
NHD11-01	0	0	2	0	0	0
NHD11-02	0	0	1	1	0	0
NHD11-04	0	0	8	0	0	0
NHD11-05	0	0	0	0	2	0
NHD11-06	0	0	1	1	0	0
NHD11-07	0	1	0	1	5	0
LPS-09-01	0	0	0	0	7	0
LPS-09-2	0	0	0	0	1	0
LPS-09-03	0	0	0	0	3	0
LSGB11-L1-02	1	2	0	0	6	0
LSGB11-L1-06	0	1	0	0	8	0

Data Repository 3, continued.

Sample number	Phytolith morphotype (compound variable)					Phytolith population total
	SAF-1 (CHLOR)	SA-1 (CHLOR)	SA-3 (BAMB/B)	SA-5 (CHLOR)	Bl-13 (BAMB/B)	
LP11-02	0	0	0	0	0	299
LP11-03	0	2	0	0	0	261
LP11-04	0	15	0	2	0	300
LP11-05	0	7	1	1	0	527
LP11-06	0	4	0	3	0	527
LP11-08	0	7	0	0	0	376
LP11-10	0	9	0	0	0	410
LSG11-01	0	0	0	0	0	283
LSG11-03	0	1	0	0	0	271
LSG11-04	0	0	0	0	0	345
LSG11-05	0	0	0	0	0	376
LSG11-06	0	0	0	0	0	390
LSGB11-04	0	0	0	0	0	283
LSGB11-07	0	0	0	0	0	282
LSGB11-11	0	0	0	0	0	306
LSGB11-12	0	0	0	0	0	253
MR11-07	/	/	/	/	/	n/a
MR11-16	/	p	/	/	/	n/a
MR11-23	/	/	/	/	/	n/a
MR11-25	0	0	0	0	0	381
MR11-28	0	0	0	0	0	271
MR11-29	p	/	/	/	/	n/a
NHD11-01	0	0	0	0	0	339
NHD11-02	0	0	0	0	0	250
NHD11-04	0	0	0	0	1	373
NHD11-05	0	0	0	0	0	370
NHD11-06	0	0	0	0	0	423
NHD11-07	1	0	0	0	0	391
LPS-09-01	0	1	0	0	0	414
LPS-09-2	0	4	0	0	0	228
LPS-09-03	0	4	0	0	0	263
LSGB11-L1-02	0	2	0	1	0	249
LSGB11-L1-06	3	0	0	0	0	260

Data Repository 3, continued.

Sample number	diatoms	sponge spicules	chrysophyte	DSC total	unknown	Total biosilica
LP11-02	0	0	0	0	10	309
LP11-03	0	0	0	0	3	264
LP11-04	0	0	0	0	71	371
LP11-05	0	0	0	0	99	626
LP11-06	0	1	1	2	16	545
LP11-08	0	1	2	3	27	406
LP11-10	0	0	0	0	23	433
LSG11-01	0	0	0	0	10	293
LSG11-03	0	1	1	2	16	289
LSG11-04	1	0	1	2	21	368
LSG11-05	0	1	0	1	3	380
LSG11-06	0	2	0	2	14	406
LSGB11-04	9	6	0	15	60	358
LSGB11-07	0	1	0	1	18	301
LSGB11-11	1	2	0	3	15	324
LSGB11-12	1	0	2	3	100	356
MR11-07	p	/	/	p	/	p
MR11-16	p	p	/	p	p	p
MR11-23	/	p	/	p	/	p
MR11-25	10	2	0	12	7	400
MR11-28	1	0	0	1	45	317
MR11-29	p	p	/	p	p	p
NHD11-01	0	0	0	0	10	349
NHD11-02	0	2	0	2	19	271
NHD11-04	0	0	0	0	5	378
NHD11-05	0	0	0	0	6	376
NHD11-06	0	0	0	0	4	427
NHD11-07	0	1	0	1	0	392
LPS-09-01	1	1	0	2	5	421
LPS-09-2	0	0	1	1	14	243
LPS-09-03	0	0	0	0	15	278
LSGB11-L1-02	1	7	0	8	20	277
LSGB11-L1-06	0	3	1	4	30	294

Data Repository 4. Raw phytolith counts grouped by plant category. FI total and GSSC (in bold) were used for vegetation reconstruction. *p = present but not part of count.

Sample number	Meter level	Plant category*						
		FI Total	Palm	FI-palm	**GSSC**	Potential Grass	Sedge	OTH total
LP11-02	3.5	197	0	197	10	0	0	102
LP11-03	5.8	181	6	175	21	0	0	62
LP11-04	8.7	134	28	106	86	0	0	151
LP11-05	10.7	94	17	77	107	0	0	428
LP11-06	0.4	158	17	141	50	0	1	334
LP11-08	2.5	157	16	141	55	0	0	191
LP11-10	3.1	139	14	125	63	0	0	231
LSG11-01	1.6	105	8	97	103	1	0	84
LSG11-03	7.7	46	8	38	151	7	1	83
LSG11-04	8.5	101	1	100	122	0	0	147
LSG11-05	13.2	134	6	128	73	0	0	172
LSG11-06	15.8	191	18	173	26	0	0	187
LSGB11-04	4.2	207	76	131	7	0	0	130
LSGB11-07	8.9	161	16	145	41	0	0	98
LSGB11-11	13.1	198	27	171	13	0	0	111
LSGB11-12	14.5	162	19	143	45	2	0	146
MR11-07	9.3	p	/	p	/	p	/	p
MR11-16	24.3	p	p	p	p	/	/	p
MR11-23	41.1	p	p	p	/	/	/	p
MR11-25	43.7	160	32	128	44	0	0	184
MR11-28	59.6	180	8	172	21	0	0	115
MR11-29	65.3	p	/	p	p	/	/	p
NHD11-01	3.5	285	3	282	14	0	0	50
NHD11-02	3.3	202	7	195	19	0	0	48
NHD11-04	6.7	152	6	146	66	0	0	160
NHD11-05	7.1	162	6	156	27	13	0	174
NHD11-06	6.7	165	4	161	50	0	0	212
NHD11-07	11.6	187	132	55	16	2	0	186
LPS-09-01	~2.3	105	6	99	96	0	0	219
LPS-09-02	~3.2	183	10	173	30	0	0	30
LPS-09-03	~3.9	159	11	148	37	0	3	83
LSGB-L1-02	13.7	172	17	155	28	0	0	68
LSGB-L1-06	13.7	171	13	158	29	7	0	83

Data Repository 5. Percent frequency (of total biosilica) of biosilica morphotypes from the Middle Chadronian-Orellan, Sage Creek Basin, Montana. *p = present but not part of count, *Other = unknown morphotypes + nondiagnostic phytoliths

Sample number	Meter level	Plant category*							Dia-toms	Sponge spicules	Chryso phyte	DSC total
		FI Total	Palm	FI-palm	GSSC	Poten-tial grass	Sedge	*Other				
LP11-02	3.5	63.75	0.00	63.75	3.24	0.00	0.00	33.01	0.00	0.00	0.00	0.00
LP11-03	5.8	68.56	2.27	66.29	7.95	0.00	0.00	23.48	0.00	0.00	0.00	0.00
LP11-04	8.7	36.12	7.55	28.57	23.18	0.00	0.00	40.70	0.00	0.00	0.00	0.00
LP11-05	10.7	14.94	2.70	12.24	17.01	0.00	0.00	68.04	0.00	0.00	0.00	0.00
LP11-06	0.4	28.99	3.12	25.87	9.17	0.00	0.18	61.28	0.00	0.18	0.18	0.37
LP11-08	2.5	38.67	3.94	34.73	13.55	0.00	0.00	47.04	0.00	0.25	0.49	0.74
LP11-10	3.1	32.10	3.23	28.87	14.55	0.00	0.00	53.35	0.00	0.00	0.00	0.00
LSG11-01	1.6	35.84	2.73	33.11	35.15	0.34	0.00	28.67	0.00	0.00	0.00	0.00
LSG11-03	7.7	15.86	2.76	13.10	52.07	2.41	0.34	28.62	0.00	0.34	0.34	0.69
LSG11-04	8.5	27.15	0.27	26.88	32.80	0.00	0.00	39.52	0.27	0.00	0.27	0.54
LSG11-05	13.2	35.26	1.58	33.68	19.21	0.00	0.00	45.26	0.00	0.26	0.00	0.26
LSG11-06	15.8	47.04	4.43	42.61	6.40	0.00	0.00	46.06	0.00	0.49	0.00	0.49
LSGB11-04	4.2	57.66	21.17	36.49	1.95	0.00	0.00	36.21	2.51	1.67	0.00	4.18
LSGB11-07	8.9	53.49	5.32	48.17	13.62	0.00	0.00	32.56	0.00	0.33	0.00	0.33
LSGB11-11	13.1	60.92	8.31	52.62	4.00	0.00	0.00	34.15	0.31	0.62	0.00	0.92
LSGB11-12	14.5	45.25	5.31	39.94	12.57	0.56	0.00	40.78	0.28	0.00	0.56	0.84
MR11-07	9.3	4.76	0.00	4.76	0.00	0.00	0.00	85.71	9.52	0.00	0.00	9.52
MR11-16	24.3	46.98	32.97	14.01	3.57	0.00	0.00	41.48	4.40	3.57	0.00	7.97
MR11-23	41.1	28.81	27.12	1.69	0.00	0.00	0.00	47.46	0.00	23.73	0.00	23.73
MR11-25	43.7	40.00	8.00	32.00	11.00	0.00	0.00	46.00	2.50	0.50	0.00	3.00
MR11-28	59.6	56.78	2.52	54.26	6.62	0.00	0.00	36.28	0.32	0.00	0.00	0.32
MR11-29	65.3	23.66	0.00	23.66	1.44	0.00	0.00	62.55	3.91	8.44	0.00	12.35
NHD11-01	3.5	74.54	2.58	71.96	7.01	0.00	0.00	17.71	0.00	0.74	0.00	0.74
NHD11-02	3.3	81.66	0.86	80.80	4.01	0.00	0.00	14.33	0.00	0.00	0.00	0.00

Data Repository 5, continued.

Sample number	Meter level	Plant category*							Phyto-lith Total	Dia-tom	Sponge spicules	Chryso phyte	DSC total
		FI Total	Palm	FI-palm	GSSC	Poten-tial grass	Sedge	Other					
NHD11-05	7.1	38.64	0.94	37.70	11.71	0.00	0.00	11.71	49.65	0.00	0.00	0.00	0.00
NHD11-06	6.7	43.09	1.60	41.49	7.18	3.46	0.00	10.64	46.28	0.00	0.00	0.00	0.00
NHD11-07	11.6	47.70	33.67	14.03	4.08	0.51	0.00	4.59	47.45	0.00	0.26	0.00	0.26
LPS-09-01	~2.3	24.88	1.42	23.46	22.75	0.00	0.00	22.75	51.90	0.24	0.24	0.00	0.47
LPS-09-02	~3.2	75.00	4.10	70.90	12.30	0.00	0.00	12.30	12.30	0.00	0.00	0.41	0.41
LPS-09-03	~3.9	56.38	3.90	52.48	13.12	0.00	1.06	14.18	29.43	0.00	0.00	0.00	0.00
LSGB-L1-02	13.7	62.32	6.16	56.16	10.14	0.00	0.00	10.14	24.64	0.36	2.54	0.00	2.90
LSGB-L1-06	13.7	59.93	4.23	55.70	9.45	2.28	0.00	11.73	27.04	0.00	0.98	0.33	1.30

Data repository 6. Plant category data (as percent of total phytolith population) used to infer vegetation types from the Middle Chadronian-Orellan, Sage Creek Basin, Montana.

Sample number	Meter level	Plant category							
		FI (total)	Palm	FI-palm	GSSC	Potential grass	Sedge	Total grass	OTH
LP11-02	3.5	63.75	0.00	63.75	3.24	0.00	0.00	3.24	33.01
LP11-03	5.8	68.56	2.27	66.29	7.95	0.00	0.00	7.95	23.48
LP11-04	8.7	36.12	7.55	28.57	23.18	0.00	0.00	23.18	40.70
LP11-05	10.7	14.94	2.70	12.24	17.01	0.00	0.00	17.01	68.04
LP11-06	0.4	29.10	3.13	25.97	9.21	0.00	0.18	9.39	61.51
LP11-08	2.5	38.96	3.97	34.99	13.65	0.00	0.00	13.65	47.39
LP11-10	3.1	32.10	3.23	28.87	14.55	0.00	0.00	14.55	53.35
LSG11-01	1.6	35.84	2.73	33.11	35.15	0.34	0.00	35.49	28.67
LSG11-03	7.7	15.97	2.78	13.19	52.43	2.43	0.35	55.21	28.82
LSG11-04	8.5	27.30	0.27	27.03	32.97	0.00	0.00	32.97	39.73
LSG11-05	13.2	35.36	1.58	33.77	19.26	0.00	0.00	19.26	45.38
LSG11-06	15.8	47.28	4.46	42.82	6.44	0.00	0.00	6.44	46.29
LSGB11-04	4.2	60.17	22.09	38.08	2.03	0.00	0.00	2.03	37.79
LSGB11-07	8.9	53.67	5.33	48.33	13.67	0.00	0.00	13.67	32.67
LSGB11-11	13.1	61.49	8.39	53.11	4.04	0.00	0.00	4.04	34.47
LSGB11-12	14.5	45.63	5.35	40.28	12.68	0.56	0.00	13.24	41.13
MR11-25	43.7	41.24	8.25	32.99	11.34	0.00	0.00	11.34	47.42
MR11-28	59.6	56.96	2.53	54.43	6.65	0.00	0.00	6.65	36.39
NHD11-01	3.5	81.66	0.86	80.80	4.01	0.00	0.00	4.01	14.33
NHD11-02	3.3	75.09	2.60	72.49	7.06	0.00	0.00	7.06	17.84
NHD11-04	6.7	40.21	1.59	38.62	17.46	0.00	0.00	17.46	42.33
NHD11-05	7.1	43.09	1.60	41.49	7.18	3.46	0.00	10.64	46.28
NHD11-06	6.7	38.64	0.94	37.70	11.71	0.00	0.00	11.71	49.65
NHD11-07	11.6	47.83	33.76	14.07	4.09	0.51	0.00	4.60	47.57
LPS-09-01	~2.3	25.00	1.43	23.57	22.86	0.00	0.00	22.86	52.14
LPS-09-02	~3.2	75.31	4.12	71.19	12.35	0.00	0.00	12.35	12.35
LPS-09-03	~3.9	56.38	3.90	52.48	13.12	0.00	1.06	14.18	29.43
LSGB-L1-02	13.7	64.18	6.34	57.84	10.45	0.00	0.00	10.45	25.37
LSGB-L1-06	13.7	60.73	4.29	56.44	9.57	2.31	0.00	11.88	27.39

Data repository 7. Plant category data (as percent of total FIs and GSSCs) used to infer vegetation types for the Middle Chadronian-Orellan, Sage Creek Basin, Montana.

Sample number	Meter level	Plant category, % of FI+GSSC		FI+GSSC count	Phytolith total
		FI	GSSC		
LP11-02	3.5	95.17	4.83	207	309
LP11-03	5.8	89.60	10.40	202	264
LP11-04	8.7	60.91	39.09	220	371
LP11-05	10.7	46.77	53.23	201	629
LP11-06	0.4	75.96	24.04	208	545
LP11-08	2.5	74.06	25.94	212	406
LP11-10	3.1	68.81	31.19	202	433
LSG11-01	1.6	50.24	49.76	209	293
LSG11-03	7.7	22.55	77.45	204	290
LSG11-04	8.5	45.29	54.71	223	372
LSG11-05	13.2	64.73	35.27	207	380
LSG11-06	15.8	88.02	11.98	217	406
LSGB11-04	4.2	96.73	3.27	214	359
LSGB11-07	8.9	79.70	20.30	202	301
LSGB11-11	13.1	93.84	6.16	211	325
LSGB11-12	14.5	77.51	22.49	209	358
MR11-25	43.7	78.43	21.57	204	400
MR11-28	59.6	89.55	10.45	201	317
NHD11-01	3.5	95.32	4.68	299	349
NHD11-02	3.3	91.40	8.60	221	271
NHD11-04	6.7	69.72	30.28	218	378
NHD11-05	7.1	80.20	19.80	202	376
NHD11-06	6.7	76.74	23.26	215	427
NHD11-07	11.6	91.22	8.78	205	392
LPS-09-01	~2.3	52.24	47.76	201	422
LPS-09-02	~3.2	85.92	14.08	213	244
LPS-09-03	~3.9	81.12	18.88	196	282
LSGB-L1-02	~13.7	86	14	200	276
LSGB-L1-06	~13.7	83.63636	16.36364	220	307